JOHANNES KEPLER
UNIVERSITÄT LINZ
Netzwerk für Forschung, Lehre und Praxis

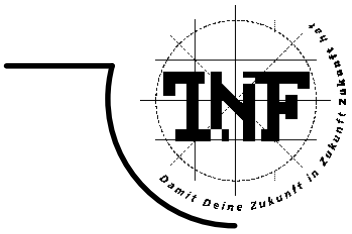

Free-form Optimization of Electric Machines based on Shape Derivatives

MASTERARBEIT

zur Erlangung des akademischen Grades

DIPLOMINGENIEURIN

im Masterstudium

INDUSTRIEMATHEMATIK

Angefertigt am *Institut für Numerische Mathematik*

Betreuung:

A. Univ. Prof. Dipl. Ing. Dr. Walter Zulehner

Eingereicht von:

Elisabeth Frank

Linz, Jänner 2010

Abstract

Shape optimization problems have many areas of application such as aerospace, structural and automotive engineering for instance. The task is to determine the optimal shape of a body insofar as it minimizes a certain cost functional subject to given constraints. The underlying work discusses the optimization of the power output of a rotating electric machine by finding the optimal motor geometry referring to the shape of the cogs in the stator.

The simulation of the motor generates a nonlinear magnetic field problem described by the Maxwell's equations. This system of partial differential equations is reduced to a $2D$ scalar partial differential equation, also referred to as magnetostatic vector potential formulation. The obtained nonlinear elliptic partial differential equation stated on the motor is the optimization constraint. Physical laws provide the boundary and interface conditions for a complete boundary value problem, which is rewritten in the variational formulation.

With differentiation formulas derived for domain and boundary integrals, the cost functional as well as both sides of the variational problem is differentiated with respect to the geometry of the motor. Now, the resulting shape gradient of the cost functional does not just depend on the geometry and the solution of the original boundary value problem, like the cost functional itself. It is furthermore a function of the so-called shape derivative which solves the differentiated linear boundary value problem.

The considered shape changes of the motor are caused by variation of defined design parameters. The new, differentiated boundary value problem includes a geometric quantity related to the modification of the motor design, which is derived for each design parameter in this work.

Both boundary value problems are solved by a simulation program that uses finite element discretization, developed by Dr. Clemens Pechstein. Numerical tests show that the derived approach could be a valuable method to compute gradient information.

Kurzfassung

Formoptimierungsprobleme werden in vielen Gebieten eingesetzt, wie zum Beispiel in der Luftfahrt, der Bautechnik und im Automobilbau. Die Aufgabe besteht darin, die optimale Form eines Körpers insofern zu bestimmen, als dass ein bestimmtes Zielfunktional unter gegebenen Nebenbedingungen minimal wird. Die vorliegende Diplomarbeit behandelt die Optimierung der Motorleistung einer rotierenden elektrischen Maschine durch Ermittlung des optimalen Motordesigns in Bezug auf die Zähne im Stator.

Die Simulation elektrischer Motoren erzeugt ein nichtlineares Magnetfeldproblem, das durch die Maxwell-Gleichungen beschrieben wird. Dieses System partieller Differentialgleichungen kann zu einer skalaren partiellen Differentialgleichung in $2D$ vereinfacht werden, welche auch als magnetostatische Vektorpotential-Formulierung bezeichnet wird. Die resultierende nichtlineare elliptische partielle Differentialgleichung bildet die Nebenbedingung der Optimierung. Physikalische Gesetze liefern die Rand- und Interfacebedingungen für ein Randwertproblem, welches in die Variationsformulierung gebracht wird.

Mithilfe der hergeleiteten Ableitungsformeln für Volumen- und Randintegrale werden sowohl das Zielfunktional, als auch beide Seiten des Variationsproblems, bezüglich der Motorgeometrie differenziert. Der resultierende Formgradient des Zielfunktionals hängt, im Gegensatz zum Zielfunktional selbst, nicht nur von der Geometrie und der Lösung des ursprünglichen Randwertproblems ab, sondern auch von der sogenannten Formableitung. Diese ist als Lösung des differenzierten, linearen Randwertproblems gegeben.

Die betrachteten Formveränderungen des Motors werden durch Variation festgelegter Designparameter verursacht. Das neue, differenzierte Randwertproblem enthält eine geometrische Größe, die mit der Modifikation des Motordesigns zusammenhängt. Diese wird in der Arbeit für alle betrachteten Designparameter hergeleitet.

Beide Randwertprobleme werden mit einem von Dr. Clemens Pechstein entwickelten Simulationsprogramm mit Finite-Elemente Diskretisierung gelöst. Numerische Tests bestätigen, dass die vorgestellte Methode für die Gradientenberechnung durchaus wertvoll sein könnte.

Acknowledgements

First of all, I would like to thank Professor Walter Zulehner for supervising my diploma thesis, especially for giving me the chance to treat a very application-oriented topic of high industrial interest and organizing financial support. I am grateful for the guidance, the prompt answers to any of my concerns and his great commitment in analyzing the numerical results.

My special thanks go to Dr. Clemens Pechstein, who developed the simulation program ParNFB that was used for all computations. I appreciate his help in programming and his availability for discussions at short notice. Furthermore, I thank Dr. Clemens Pechstein for his patience, his effort in debugging and his valuable time.

Most of all I want to thank my family for the mental backup and their support concerning all needs beyond this work.

This work has been carried out at the Institute of Computional Mathematics, JKU Linz, in cooperation with ACCM (Austrian Center of Competence in Mechatronics), a K2-Center of the COMET/K2 program of the Federal Ministry of Transport, Innovation, and Technology, and the Federal Ministry of Economics and Labour, Austria.

Moreover I acknowledge the Institute of Computational Mathematics at the Johannes Kepler University of Linz, chaired by Prof. Ulrich Langer, for the technical support.

Elisabeth Frank
Linz, January 19, 2010

Contents

1 Introduction **1**

2 Problem Formulation **4**

2.1 Motor design 4

2.2 The Optimization Problem 6

2.3 Physical background 7

2.4 Mathematical Model 10

3 Geometry **14**

3.1 Shape Variation 14

3.2 Design Parameters 16

3.3 Normal Velocity Component 19

3.3.1 Variation of the ratio ρ 20

3.3.2 Variation of the x-coordinate of M_1 22

3.3.3 Summary 27

4 Introduction to Shape Derivatives **29**

4.1 Domain Integrals 30

4.2 Boundary Integrals 35

4.2.1 Tangential Operators and Formulas 35

4.2.2 Differentiation Formula 37

5 The Main Problem **41**

5.1 The Cost Functional and its Gradient 41

5.1.1 Specification of the functional 41

5.1.2 Formulation of the cost functional 42

5.1.3 Computation of the gradient 43

5.2 Differentiation of the Variational Problem 45

6 Numerical Results **53**

6.1 Simplified Test Problem 53

6.1.1 Problem Description 54

6.1.2 Boundary value problem for u 54

6.1.3 Boundary value problem for the shape derivative 56

6.1.4 The cost functional and its gradient 59

6.1.5 Results 61

6.2 Original Problem 64

6.2.1 Problem Description 64

6.2.2 Results 67

7 Conclusion and Future Work **70**

Bibliography **73**

List of Figures

2.1 Motor layout in $2D$ 5
2.2 Detailed structure of rotor (left) and stator (right) 6

3.1 Domain transformation by map T_t 15
3.2 Motor design with cog formed by circles 17
3.3 Zoomed view of first coil sector 18
3.4 Coil sector with gray shaded cog 19
3.5 Transformation at variation of ratio 21
3.6 Geometrical change at variation of $x_{M,1}$ 23
3.7 Particle displacement at variation of $x_{M,1}$ 24

6.1 Domain for the test problem 54
6.2 Transformation at variation of the radius R 58
6.3 Error in the state variable u 61
6.4 Error in the shape derivative u' 62
6.5 Error in the shape derivative u' when the variational problem is not well-defined in $H^1(\Omega)$ 62
6.6 Comparison of computed and exact cost functional 63
6.7 Comparison of computed and exact gradient of the cost functional . . . 64
6.8 Motor subdomains for simulation 65
6.9 Current density in the motor 66
6.10 State variable u at ratio 1 67
6.11 Shape derivative u' at ratio 1 68
6.12 Development of the cost functional 69
6.13 Comparison of differentiation methods 69

List of Notations

In this thesis the index e always refers to exact solutions and functionals.

Notations related to differentiation

f'	shape derivative of f
$\dot{f}$	material derivative of f
$\frac{\partial f}{\partial t}$	partial derivative of f w.r.t. t
$Df = \left(\frac{\partial f, i}{\partial x_j}\right)_{\substack{i=1,\dots m \\ j=1,\dots n}}$	Jacobian of $f : \mathbb{R}^n \to \mathbb{R}^m$
$D_x f = \left(\frac{\partial f}{\partial x_1}, \dots, \frac{\partial f}{\partial x_n}\right)$	derivative of $f : \mathbb{R}^n \to \mathbb{R}$ w.r.t. $x \in \mathbb{R}^n$ (row vector)
$D_y f = \frac{\partial f}{\partial y}$	derivative of $f : \mathbb{R}^n \to \mathbb{R}$ w.r.t. $y \in \mathbb{R}$ (scalar)
∇f	gradient of $f : \mathbb{R}^n \to \mathbb{R}$ w.r.t. $x \in \mathbb{R}^n$ (column vector)
$\nabla_\Gamma f$	tangential gradient of $f : \mathbb{R}^n \to \mathbb{R}$ w.r.t. $x \in \mathbb{R}^n$
$\operatorname{div} f$	divergence of f
$\operatorname{div}_\Gamma f$	tangential divergence of f
$\operatorname{curl} f = \nabla \times f$	curl of $f : \mathbb{R}^3 \to \mathbb{R}^3$
Δf	Laplacian of $f : \mathbb{R}^n \to \mathbb{R}$
$dJ,\ \frac{d}{dt} J\big\vert_{t=0}$	Eulerian derivative of functional J
DJ	Shape gradient of functional J

Notations related to linear algebra

I	identity matrix
id	identity operator
$f \circ g = f(g)$	composition
A^{-1}	inverse of matrix A
A^T	transpose of matrix A
$\mathrm{tr}\, A$	trace of matrix A
$\mathrm{adj}(A)$	adjugate of matrix A

Notations related to spaces, norms and scalar products

$L^2(\Omega)$	space of square integrable functions on Ω
$V = H^1(\Omega)$	Sobolev space of L^2-functions with square integrable first derivative
$V_0 = H_0^1(\Omega)$	functions from V that vanish on Dirichlet boundaries
$\|.\|$ or $\|.\|_{l_2}$	Euclidean norm
$f \cdot g = \sum_{i=1}^n f_i g_i$	inner product of vector-valued functions f, g
$a^T b$	scalar product of column vectors $a, b \in \mathbb{R}^n$
$f \times g$	cross product of vector-valued functions f, g

Notations related to Variational Problems

$\bar{\Omega} = \bigcup_{i=1}^N \bar{\Omega}^{(i)}$	heterogeneous bounded domain in $\mathbb{R}^n$
$\Gamma = \partial\Omega$	boundary of Ω
$\Gamma^{(i,j)}$	interface between two subdomains $\Omega^{(i)}$ and $\Omega^{(j)}$
$\vec{n}$, n	outer unit normal vector
u_i, $M^{(i)}$	restriction of u and M, respectively, to $\Omega^{(i)}$
$v \in V_0$	test function
$a(.,.)$	bilinear form
$< .,. >$	linear form

Notations related to electromagnetic fields

$\mathbf{H}$	magnetic field strength
$\mathbf{E}$	electric field strength
$\mathbf{B}$	magnetic flux density
$\mathbf{D}$	electric flux density
$\mathbf{J}$	electric current density
$\mathbf{M}$	permanent magnetization
$\mathbf{B}_r$	magnetic remanence
$\mathbf{A}$	vector potential
$M_\perp$	perpendicular to $\mathbf{M}$ in $2D$
μ	magnetic permeability
ϵ	electric permittivity
σ	electric conductivity
ρ	electric charge density
ν	magnetic reluctivity

Notations related to the cost functional

$\mathcal{J}$	cost functional
T	(magnitude of) torque, simplified cost functional
$\vec{T}$	torque vector
I	electric current
R	resistance
ω	rotational frequency
$\vec{\vec{\sigma}}$	Maxwell Tensor
$\vec{F}$	force vector
$\vec{r}$	lever arm vector
Q	symmetric matrix
Γ_0	outer boundary of air gap

Notations related to geometry

Indices:

0	referring to initial geometry
t	referring to transformed geometry
1	referring to outer circle defining cog
2	referring to inner circle defining cog

d	vector of design parameters
n	number of design parameters
t	amount of change in design parameter
X	Lagrangean coordinate
x	Eulerian coordinate
T_t	transformation
V	Eulerian velocity field
v_n	normal component of Eulerian velocity field
s	length of particle displacement
R	rotor radius
R_0	radius of integration curve
ρ	ratio of radii, design parameter
r	radius of circle defining cog
$M = (x, y)$	center of circle defining cog
$\bar{M}$	reflection of M
B	contact point of tangent circles

Chapter 1

Introduction

This thesis deals with the shape optimization of an electric motor. The topic was motivated by a cooperation with the ACCM (Austrian Center of Competence in Mechatronics) and is based on results obtained in the project seminar in computational mathematics held in the summer semester 2008 at JKU Linz.

Shape optimization problems are concerned with finding the optimal design with respect to a given cost functional, usually subject to an underlying partial differential equation. The numerical solution of such problems requires information about the gradient of the cost functional, which can be approximated by difference quotients. However, this method has some drawbacks like the accuracy of the approximation, computational costs and the problem of determining an appropriate stepsize.
The underlying thesis presents an approach of computing the exact gradient of the cost functional with respect to the geometry. The involved tasks are worked out for the case of a rotating electric machine.

The machine considered for the optimization more precisely represents a PMSM (Permanent Magnet Synchronous Motor). The rotor of this motor type is permanently magnetized, coils conducted with current are situated in the stator. In contrast to other machines, the magnetic field in the stator is not generated electrically but by the permanent magnets in the rotor.
Thus, the excitation does not require electric power which increases the degree of efficiency of the machine. Moreover, a PMSM is brushless without a commutator making the machine low-maintenance, resistant and causing less wear.
Permanent magnetic motors have gained in importance in many fields of application.

For instance, they are used in machine tools, different industrial robots, production machines, air conditioners, pipe systems and several home appliances.

This thesis aims to present the treatment of a shape optimization problem from the very first step. Particular attention is paid to the meaning of the design of a physical domain as an optimization variable and the differentiation of functionals with respect to that domain. The latter is a challenging task because the optimization constraint is a partial differential equation (PDE) which is defined on the considered domain.
The derivation of the differentiation formulas is mainly based on [15]. The presentation in this work will be formal, i.e. it is correct provided that all needed data are sufficiently smooth. Regularity assumptions and functional analytic aspects are discussed in [15] and [4].
Moreover we omit a detailed description of all physical laws and relations. This part of the thesis is limited to a short introduction of the main statements needed to derive the mathematical model.

The thesis is organized as follows:

In chapter 2 we first introduce the initial design of the given permanently magnetized motor and formulate the shape optimization problem. The PDE constraint is derived from the Maxwell's equations that are used to describe electromagnetic field problems. Appropriate boundary and interface conditions lead to a nonlinear boundary value problem on the motor.

Chapter 3 identifies design parameters and visualizes the shape changes resulting from their variation. Furthermore the normal velocity component, which appears in the differentiation formulas of chapter 4, is calculated for each design parameter.

The shape differentiation of functionals consisting of domain or boundary integrals is explained in chapter 4. Important types of derivatives, such as the material or the shape derivative, are defined and used to derive general expressions for derivatives with respect to a geometric domain.

In chapter 5 we apply the differentiation theory worked out earlier to the main problem. The formulas yield the shape gradient of the cost functional needed for the optimization and we obtain a second boundary value problem by differentiating both sides of the

original one, which was derived in chapter 2. The solutions of both problems are required to evaluate the gradient of the cost functional.

Finally, chapter 6 provides the numerical results computed with a simulation program developed by Dr. Clemens Pechstein. On the basis of a simplified test problem with a known exact solution, the programming code is verified. For the original model problem a comparison of the difference quotient and the computed shape gradient shows that the presented method is reasonable.

In chapter 7 we evaluate the differentiation method using shape derivatives in comparison to approximations by difference quotients, regarding computational costs and accuracy.

Chapter 2

Problem Formulation

This chapter presents the PDE constrained shape optimization problem and derives a mathematical problem formulation. It is structured in the following way:
In section 2.1, we illustrate the initial geometry of the motor to be optimized. A formal specification of the optimization problem is provided in section 2.2. In section 2.3 we briefly present the underlying physical engineering problem on the basis of fundamental relations in electromagnetics and derive the magnetostatic vector potential formulation, which is simplified under consideration of relevant problem properties and admissible assumptions in section 2.4.

2.1 Motor design

The considered synchronous motor is part of a - initially given in $3D$ - rotating electric machine. For symmetry reasons, the x_3-direction can be neglected leading to a $2D$ model.

Figure 2.1 sketches the reduced motor in the x_1x_2-plane. The innermost circle defines the motor center which is orbited by the rotor, i.e. the rotation axis goes through the midpoint. The surrounding circular ring represents the rotor, whereas its enclosing narrow layer identifies the airgap inbetween the rotor and the fixed stator. The next two rings, describing the coil area and an iron layer, belong to the stator. The outermost district forms a virtual layer of air that will be needed for the mathematical problem description.

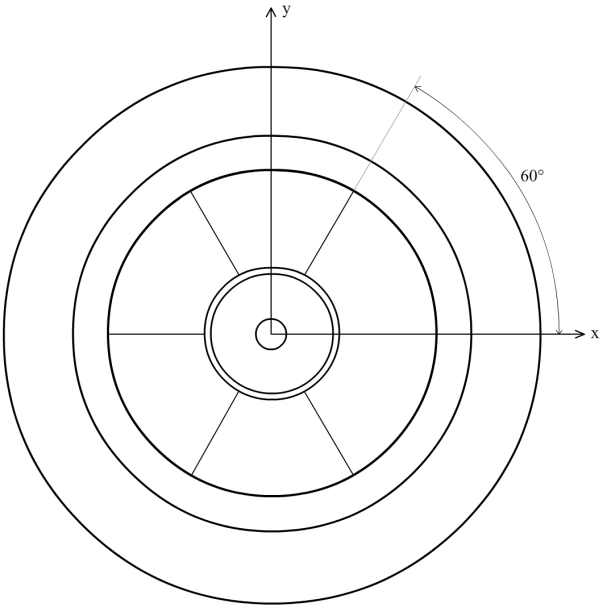

Figure 2.1: Motor layout in $2D$

Both the rotor and the stator are separately viewed in figure 2.2 The left picture shows the detailed structure of the rotor, the stator is displayed on the right side. Note that in this graphic, the two motor parts are not proportional in size to one another, the rotor actually fits inside the stator.
The inner disk of the rotor consists of iron, the outer circular ring constitutes four permanent magnets. The arrows stand for the magnetization direction and show that we are dealing with parallel magnetization. In each quadrant, the magnetization points in the direction of the bisecting line, with alternating sign.
The stator is composed of coils and an enclosing iron ring. The coil layer is divided into the six segments A_1 to A_6 which identify the part of the rotor that is conducted by current. The outer ring is made of iron like the inner part of the rotor.

With geometric variables like various diameters, the geometry of the motor can be parameterized. Detailed information on the motor dimensions that are used for the numerical tests is given on page 65. This part of the geometry is fixed for the optimization.
Each of the coil districts A_1 to A_6 actually represents a cog lying in the middle of

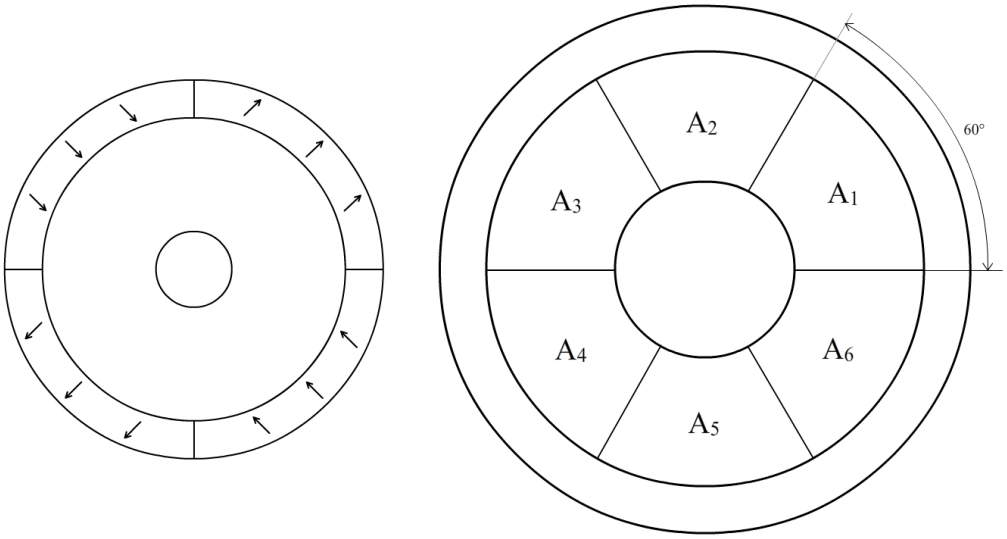

Figure 2.2: Detailed structure of rotor (left) and stator (right)

a coil area. Coils of wire are wound around the cogs which are connected with the surrounding iron ring. In chapter 3, we will split the coil segments to obtain a stator consisting of an iron ring with six cogs. The goal is to find the best shape of the cogs which leads to the underlying shape optimization problem.

2.2 The Optimization Problem

The goal is to find the optimal design of the motor in such a way that the machine power is maximized. Mathematically, the problem writes as follows:

$$\begin{aligned} &\min_{d\in\mathbb{R}^n} \mathcal{J}(d, u(d)) \\ &\text{s.t.: } u(d) \text{ solves nonlinear elliptic PDE} \\ &\qquad \underline{d}_i \le d_i \le \overline{d}_i \qquad \forall i \in \{1, 2, \dots n\} \end{aligned} \tag{2.1}$$

with

$\mathcal{J}$	cost functional
$u(d)$	state variable
d	vector of design parameters
n	number of design parameters

The cost functional $\mathcal{J}$ is the power output of the motor and depends on the motor geometry, as well as on the state variable u.
In general, u satisfies a nonlinear elliptic PDE that will be derived from the Maxwell's equations in sections 2.3 and 2.4. It describes the state of the electromagnetic behavior of the system and will be the third component of a vector potential (see section 2.4). The PDE with solution u is stated on the domain representing the motor, i.e. the state variable u itself also depends on the motor geometry.

The geometry of the motor is described by n so-called design parameters, collected in a vector d. Changes in the geometry of the motor are caused by variation of one or more design parameters.
For the optimization problem treated in this work, the design parameters correspond to the six cogs in the stator. More details will be provided in chapter 3.
The prescribed lower and upper bounds (box constraints) define the feasible region for all parameters to avoid useless shapes like cogs that do not touch the iron ring, for instance.

2.3 Physical background

The state variable u, which is required to evaluate the cost functional $\mathcal{J}$, underlies the Maxwell's equations, given by

$$\operatorname{curl} \mathbf{H} = \mathbf{J} + \frac{\partial \mathbf{D}}{\partial t} \tag{2.2}$$

$$\operatorname{curl} \mathbf{E} = -\frac{\partial \mathbf{B}}{\partial t} \tag{2.3}$$

$$\operatorname{div} \mathbf{B} = 0 \tag{2.4}$$

$$\operatorname{div} \mathbf{D} = \rho \tag{2.5}$$

with the involved electromagnetic quantities

$\mathbf{H}$	magnetic field strength
$\mathbf{E}$	electric field strength
$\mathbf{B}$	magnetic flux density or magnetic induction
$\mathbf{D}$	electric flux density or electric induction
$\mathbf{J}$	electric current density
ρ	electric charge density

The boldface notation indicates vector fields in $3D$. All introduced quantities depend on the position $\mathbf{x} = (x_1, x_2, x_3)$ and time t. This famous system of PDEs is stated in most books concerning electromagnetics. For details and explanations we refer to [7, 8, 11].

Relations between the fields are expressed via the following constitutive laws:

$$\mathbf{B} = \mu \cdot (\mathbf{H} + \mathbf{M}) \tag{2.6}$$

$$\mathbf{D} = \epsilon \mathbf{E} \tag{2.7}$$

$$\mathbf{J} = \sigma \mathbf{E} \tag{2.8}$$

with

$\mathbf{M}$	field of permanent magnetization
μ	magnetic permeability
ϵ	electric permittivity
σ	electric conductivity.

The magnetic field $\mathbf{M}$ is given by

$$\mathbf{M} = \mu \mathbf{B}_r \tag{2.9}$$

where $\mathbf{B}_r$ denotes the magnetic remanence. The material quantities μ, ϵ and σ generally are nonlinear tensors that depend on time and space. However, we concentrate on the isotropic case and therefore they are numbers.

In the following, we further investigate the magnetic permeability.
Since we neglect the effects of hysteresis, the permeability can be seen as a function of the magnitude of the magnetic field strength $|\mathbf{H}|$, leading to

$$\mathbf{B} = \mu(|\mathbf{H}|) \cdot (\mathbf{H} + \mathbf{M}).$$

Note that $\mathbf{M}$ only appears in materials that are permanently magnetized.
The permeability is furthermore defined as

$$\mu = \mu_0 \mu_r \tag{2.10}$$

with the constant permeability of vacuum $\mu_0 = 4\pi 10^{-7}$ and the relative permeability μ_r.
We distinguish linear and nonlinear materials. The best known linear material is vacuum, where the relative permeability equals 1, i.e. $\mu = \mu_0$. Permanent magnetic materials have the same permeability $\mu = \mu_0$.
In nonlinear materials, μ depends on the strength of the magnetic field. It is determined by the B-H-curve, which represents a relation of the magnetic field intensity $H = |\mathbf{H}|$ and the magnitude of the magnetic induction $B = |\mathbf{B}|$. A famous nonlinear material is iron.
In the underlying motor, the iron ring and the six cogs, as well as the rotor without the permanent magnets, are made of iron.

Now we introduce another coefficient, namely the magnetic reluctivity ν, satisfying

$$\mathbf{H} = \nu(|\mathbf{B}|)\mathbf{B} - \mathbf{M}.$$

Obviously, the reluctivity is the reciprocal of the magnetic permeability.
According to [11], electromagnetic phenomena in rotating electric machines can be described by quasi-stationary magnetic fields, meaning that $\mathbf{D}$ does not influence $\mathbf{H}$ in (2.2) and $\rho = 0$. The corresponding simplified Maxwell's equations are presented in [11]. Moreover, the magnetic fields $\mathbf{H}, \mathbf{B}$ and the current density $\mathbf{J}$ do not depend on time, which refers to the magnetostatic case. The earlier introduced Maxwell's equations (2.2) - (2.5) and constitutive laws (2.6) - (2.8) reduce to

$$\operatorname{curl} \mathbf{H} = \mathbf{J} \tag{2.11}$$

$$\operatorname{div} \mathbf{B} = 0 \tag{2.12}$$

$$\mathbf{H} = \nu(|\mathbf{B}|)\mathbf{B} - \mathbf{M}. \tag{2.13}$$

Because of (2.12), the magnetic flux density can be expressed by the *curl* of a vector potential $\mathbf{A}$:

$$\mathbf{B} = \operatorname{curl} \mathbf{A}. \tag{2.14}$$

Inserting (2.14) into (2.13), applying the *curl* operator to both sides of the equation and using (2.11) yields

$$\operatorname{curl} [\nu(|\operatorname{curl} \mathbf{A}|) \operatorname{curl} \mathbf{A}] = \mathbf{J} + \operatorname{curl} \mathbf{M}, \tag{2.15}$$

which is known as the magnetostatic vector potential formulation.

2.4 Mathematical Model

Reduction to $2D$:

Since the given motor is modelled as circular disk lying in the x_1x_2-plane, the magnetic fields $\mathbf{H}$, $\mathbf{B}$ and $\mathbf{M}$ reduce to

$$\mathbf{H} = \begin{pmatrix} H_1(x_1, x_2) \\ H_2(x_1, x_2) \\ 0 \end{pmatrix}, \qquad \mathbf{B} = \begin{pmatrix} B_1(x_1, x_2) \\ B_2(x_1, x_2) \\ 0 \end{pmatrix}, \qquad \mathbf{M} = \begin{pmatrix} M_1(x_1, x_2) \\ M_2(x_1, x_2) \\ 0 \end{pmatrix}.$$

For the *curl* of the permanent magnetization appearing in (2.15) we obtain

$$\operatorname{curl} \mathbf{M} = \begin{pmatrix} 0 \\ 0 \\ -\dfrac{\partial M_1}{\partial x_2} + \dfrac{\partial M_2}{\partial x_1} \end{pmatrix}. \tag{2.16}$$

With $B_3 = 0$ we get from (2.14) the following relation:

$$\frac{\partial A_1}{\partial x_2} - \frac{\partial A_2}{\partial x_1} = 0. \tag{2.17}$$

We conclude $\mathbf{A} = (0, 0, A_3(x_1, x_2))^T$ and substitute from now on $u := A_3$, leading to

$$\mathbf{B} = \operatorname{curl} \mathbf{A} = \begin{pmatrix} \dfrac{\partial u}{\partial x_2} \\ -\dfrac{\partial u}{\partial x_1} \\ 0 \end{pmatrix} \qquad \text{and} \qquad |\mathbf{B}| = |\nabla u|. \tag{2.18}$$

The current density $\mathbf{J}$ occurs in the coil areas on both sides of each cog. Since the coils of wire are wound around the cogs in x_3-direction, $\mathbf{J}$ is perpendicular to the magnetic fields and therefore defines a vector where only the third component is nonzero:

$$\mathbf{J} = \begin{pmatrix} 0 \\ 0 \\ J_3(x_1, x_2) \end{pmatrix}.$$

Now, by using (2.16) and (2.18), the third line of the magnetic vector potential formulation (2.15) writes as

$$-\operatorname{div}\Big(\nu(|\nabla u|)\nabla u\Big) = J_3 - \frac{\partial M_1}{\partial x_2} + \frac{\partial M_2}{\partial x_1} \tag{2.19}$$

where all appearing quantities depend on the position $\mathbf{x} = (x_1, x_2)$ in the two-dimensional space .

Continuity conditions:

In the following, we derive a boundary value problem (BVP) for u to complete the mathematical problem formulation. Let the bounded domain $\Omega \subset \mathbb{R}^3$ with boundary $\Gamma = \partial\Omega$ denote the given permanently magnetized motor. Since the motor consists of various parts of different material properties (see figure 2.1), Ω is a heterogeneous domain, i.e. $\bar{\Omega} = \bigcup_{i=1}^{N} \bar{\Omega}^{(i)}$ with nonoverlapping subdomains. To ensure physically reasonable continuity conditions between two neighboring materials, we prescribe, analogously to [2], the following interface conditions:

$$\vec{n} \cdot \left(\mathbf{B}^{(j)} - \mathbf{B}^{(i)}\right) = 0 \qquad \text{on } \Gamma^{(i,j)} \tag{2.20}$$

$$\vec{n} \times \left(\mathbf{H}^{(j)} - \mathbf{H}^{(i)}\right) = 0 \qquad \text{on } \Gamma^{(i,j)} \tag{2.21}$$

with the unit normal vector $\vec{n}$, the interface $\Gamma^{(i,j)} = \partial\Omega^{(i)} \cap \partial\Omega^{(j)}$ between two subdomains $\Omega^{(i)}$ and $\Omega^{(j)}$, the restrictions $\mathbf{B}^{(i)}$ of $\mathbf{B}$ and u_i of u to $\Omega^{(i)}$, and so forth.
In the $2D$ case, the above conditions can be reduced to

$$\begin{aligned} u_i &= u_j \qquad \text{on } \Gamma^{(i,j)} \\ -\nu_i(|\nabla u_i|)\ \nabla u_i \cdot \vec{n} + \nu_j(|\nabla u_j|)\ \nabla u_j \cdot \vec{n} &= \vec{n} \cdot M_\perp^{(i)} - \vec{n} \cdot M_\perp^{(j)} \qquad \text{on } \Gamma^{(i,j)} \end{aligned}$$

with

$$M_\perp = \begin{pmatrix} -M_2 \\ M_1 \end{pmatrix}, \tag{2.22}$$

by use of (2.13) and (2.18).
On the outer boundary Γ we postulate homogeneous Dirichlet boundary conditions, which can be seen as a magnetic isolation between the virtual layer of air representing the outermost part of the motor (cf. 2.1) and the surroundings.

Classical Formulation:

Finally, the classical formulation of the BVP for u can be stated:

Find $u : \bar{\Omega} \rightarrow \mathbb{R}$ such that

$$\begin{aligned} -\operatorname{div}\left((\nu_i(|\nabla u_i|)\nabla u_i) - M_\perp^{(i)}\right) &= J_3^{(i)} \qquad \text{in } \Omega^{(i)} && (2.23) \\ \left[u\right]_{\Gamma^{(i,j)}} &= 0 \qquad \text{on } \Gamma^{(i,j)} && (2.24) \\ \left[\nu(|\nabla u|)\ \nabla u \cdot \vec{n}\right]_{\Gamma^{(i,j)}} &= \left[M_\perp \cdot \vec{n}\right]_{\Gamma^{(i,j)}} \qquad \text{on } \Gamma^{(i,j)} && (2.25) \\ u &= 0 \qquad \text{on } \Gamma && (2.26) \end{aligned}$$

with the usual jump notation

$$\begin{aligned} \left[u\right]_{\Gamma^{(i,j)}} &:= u|_{\Omega^{(i)}}(\mathbf{x}) - u|_{\Omega^{(j)}}(\mathbf{x}) = u_i(\mathbf{x}) - u_j(\mathbf{x}) \qquad \forall \mathbf{x} \in \Gamma^{(i,j)} \\ \left[q \cdot \vec{n}\right]_{\Gamma^{(i,j)}} &:= q_i(\mathbf{x}) \cdot \vec{n}^{(i)}(\mathbf{x}) + q_j(\mathbf{x}) \cdot \vec{n}^{(j)}(\mathbf{x}) \ \ \forall \mathbf{x} \in \Gamma^{(i,j)} \end{aligned}$$

and $\vec{n}^{(i)}$, $\vec{n}^{(j)}$ denoting the outer unit normal vectors to $\Omega^{(i)}$ and $\Omega^{(j)}$, respectively.

Variational Formulation:

For the variational formulation we consider the Sobolev spaces

$$V = H^1(\Omega) = \{v \in L^2(\Omega) : \nabla v \in L^2(\Omega)\}, \qquad V_0 = \{v \in V : v = 0 \text{ on } \Gamma\}. \tag{2.27}$$

The variational formulation is obtained by multiplying both sides in (2.23) with an arbitrary testfunction $v \in V_0$ and integrating over Ω. Integration by parts for the principal part and incorporating the boundary and interface conditions (2.24)-(2.26) leads to the following variational formulation:

Find $u \in V_0$, such that

$$a(u, v) = \langle f, v \rangle \qquad \forall v \in V_0 \tag{2.28}$$

where

$$a(u, v) = \int_\Omega q(\nabla u) \cdot \nabla v \, d\Omega \qquad \text{and} \tag{2.29}$$

$$\langle f, v \rangle = \int_\Omega \Big(J_3 v + M_\perp \cdot \nabla v \Big) \, d\Omega \tag{2.30}$$

with

$$q(\nabla u) = \nu(|\nabla u|)\nabla u. \tag{2.31}$$

Chapter 3

Geometry

Contrary to ordinary optimization problems, where the arguments of the cost functional are real scalars or vectors, the cost functional $\mathcal{J}$ of the minimization problem (2.1) has the physical domain Ω as a variable. Accordingly, the optimization variable is the geometry of a domain. In order to compute the gradient of our cost functional we have to differentiate $\mathcal{J}$ with respect to Ω.

This chapter represents the geometry part of the thesis. It provides the entire geometric information required to solve the optimization problem (2.1).
The first section introduces basic principles to describe changes in the geometry of a domain. In section 3.2, we parameterize the cogs of the given electric motor, i.e. we choose design parameters to specify the curve defining the shape of the cogs. Finally, a velocity field of Ω associated with the change of design parameters is computed in section 3.3.

3.1 Shape Variation

As starting point for shape variations we consider a bounded domain $\Omega \subset \mathbb{R}^m$, $m \in \mathbb{N}$ with Lipschitz boundary $\Gamma = \partial\Omega$, consisting of material particles. This initial configuration Ω is changed into a new geometry Ω_t by mapping each material particle from its position $X \in \Omega$ to its new position $x = T_t(X) \in \Omega_t$, as illustrated in figure 3.1.

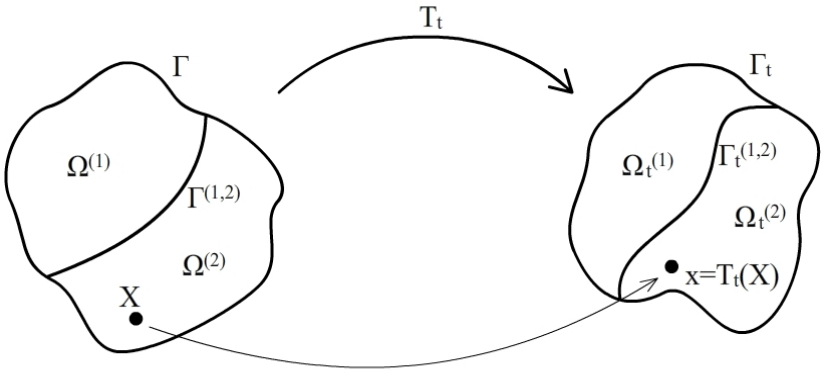

Figure 3.1: Domain transformation by map T_t

This process is realized by a one parametric family of bijective transformations

$$\begin{aligned} T_t : \mathbb{R}^m &\rightarrow \mathbb{R}^m \\ X &\rightarrow x = T_t(X) = x(t, X) \end{aligned}$$

with

$$T_t(\Omega) = \Omega_t, \qquad T_t(\partial\Omega) = \partial\Omega_t.$$

$X \in \Omega$ are called the Lagrangean coordinates of a particle whereas $x = T_t(X) \in \Omega_t$ are the Eulerian coordinates. Apparently, Ω_t is the image of the reference configuration with respect to the function T_t which maps from Lagrangean to Eulerian coordinates.

The scalar parameter $t \geq 0$ describes the amount of change of the geometry. Hence, for $t = 0$ the transformation T_t equals the identity operator and thus the initial shape remains unchanged:

$$T_0 = \mathrm{id}, \qquad T_0(\Omega) = \Omega, \qquad T_0(X) = X \qquad \forall X \in \Omega.$$

The design parameters needed in our given problem will be defined in section 3.2. Usually the parameter t is thought of as time, but here it stands for geometric quantities. Another important term to describe the transformation of a domain is the (design) velocity:

Definition 3.1 (Eulerian velocity field)**.** The Eulerian velocity field $V(t,x)$ is given by

$$V(t,x) = \frac{\partial x}{\partial t}\left(t, T_t^{-1}(x)\right).$$

We assume V is sufficiently smooth (details can be found in [4] on page 338). The Eulerian velocity field expresses the direction as well as the magnitude of the motion of a material particle occupying the position x at "time" t.

The mapping T_t and the velocity are connected via an initial value problem as stated in [10], page 34:

$$\begin{aligned} \frac{d}{dt}x(t,X) &= V(t,x(t,X)) \\ x(0,X) &= X. \end{aligned} \tag{3.1}$$

This relation signifies the dependence of the transformation on the velocity field, i.e. $x(t,X) = T_t(V)(X)$, in which we will drop the V in the following. For given velocity, the above problem determines $x(t,X)$ and thus the family of transformations T_t, and vice versa.

3.2 Design Parameters

The motor sketched in chapter 2 can be parameterized by geometric variables such as the radius of the rotor, the width of the airgap, etc. As mentioned earlier, the parametrization of the motor is not complete yet. The sectors $A_1 - A_6$ in figure 2.2 have to be further subdivided. More precisely, we have to determine a parametrization of the curve cutting each sector into three parts: the cog lying in the middle of the segment and the areas on either side of the cog, which are filled with coils of wire that are wound around the cog.

Variables appearing in the geometric description of the given machine are called *design parameters*, if they are varied to find the optimum shape of the motor, whereas all other variables are fixed. In the following, the parameters characterizing the cog curve will be referred to as design parameters or design variables.

Remark 3.2. *In the simplified test problem worked out in section 6.1, we will consider the radius of the rotor as design parameter.*

Of course, there are different ways to set up a curve defining the cogs of the motor. For example, one could prescribe a finite set of points within each sector and draw a piecewise linear function through these points. Bezier curves or other splines passing given control points represent further options.
We choose a curve which is obtained by two tangent circles as shown in figures 3.2 and 3.3. For the sake of clarity, only the cog lying in the first sector of the motor is plotted in figure 3.2. Obviously, the cogs in the other sectors are obtained by rotation.

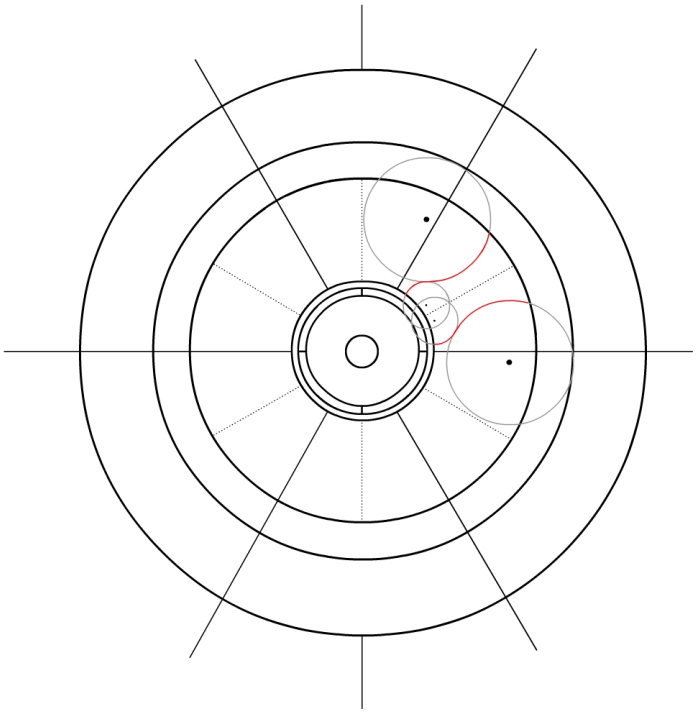

Figure 3.2: Motor design with cog formed by circles

Below, the design parameters corresponding to the red curves in figure 3.2 are introduced. Generally, a circle in $2D$ can be identified by 3 parameters (coordinates of the midpoint and the radius). Since the two circles are tangent, one parameter can be eliminated which leads to a total of 5 design parameters to consider the geometric change of the motor:

- ratio of the radii: $\rho = r_1/r_2$
- center of circle 1: $(x_{M,1}, y_{M,1})$
- center of circle 2: $(x_{M,2}, y_{M,2})$.

Circle 1 will always refer to the outward one, i.e. the circle farther from the rotor and closer to the iron ring.

Figure 3.3 provides a detailed perspective of the first motor segment. It shows the cog resulting from connected circles and points out the symmetry of a cog with respect to the midline of its sector. Thus, it is sufficient to specify two tangent circles determining the half of one cog. Reflecting and rotating them yields all curves needed to define every cog in the motor. Figure 3.4 visualizes the design of one sector obtained by the parametrization described above. This part of the motor is considered to replace the segments $A_1 - A_6$ in figure 2.2.

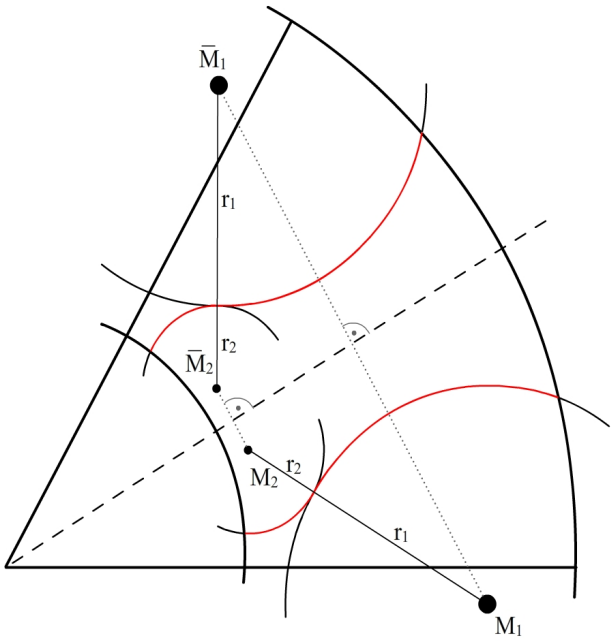

Figure 3.3: Zoomed view of first coil sector

To ensure a reasonable motor design and satisfy physical and technical requirements, the parameters have to fulfill certain restrictions. For instance, circle 1 must not

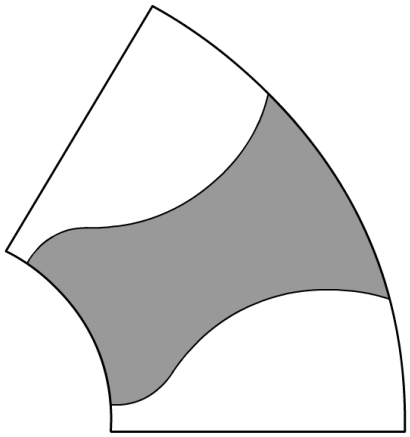

Figure 3.4: Coil sector with gray shaded cog

cut the sector-midline. This would result in a negative width of the cog. Similarly, if circle 2 exceeds its dedicated sector, i.e. cuts the sector bounds, the cogs would overlap. Moreover, both circle 1 and circle 2 have to cut their neighboring material layers. Otherwise the cogs would not be connected with the iron ring or the air gap, respectively. The set of design variables satisfying the constraints is called *feasible design*.

3.3 Normal Velocity Component

This section deals with the variation of each individual design parameter and the resulting change in the motor geometry. This means we will state for every t a one-to-one function T_t transforming the initial design Ω to Ω_t.
The map inducing the domain change is not unique. We will present one valid transformation per design parameter which we further use to compute the Eulerian velocity field and the quantity we are actually interested in: the normal component v_n of the velocity, which is given by

$$v_n(x) = V(0, x) \cdot n \tag{3.2}$$

with n denoting the unit outer normal vector to Ω, where we neglect the dependence of n on x. Chapters 4 and 5 will show that v_n appears in the differentiation formu-

las for domain and boundary integrals and thus in the differentiated boundary value problem.

Throughout this chapter, Γ_0 and Γ_t denote the boundaries of the initial domain Ω and the transformed domain Ω_t, respectively. For the computation of v_n, we only define the mapping of particles that are situated on the boundary Γ_0. We assume that a transformation $T_t : \Gamma_0 \rightarrow \Gamma_t$ can be extended consistently to the entire domain. An arbitrary extension does not influence v_n and therefore it is sufficient to define T_t on the boundary Γ_0 of Ω.

3.3.1 Variation of the ratio ρ

We start considering the ratio ρ of the two circles' radii as design parameter. Let $r_{0,1}$ and $r_{0,2}$ be the radii of the two initial circles and let ρ_0 denote their ratio, i.e. $\rho_0 = r_{0,1}/r_{0,2}$. Furthermore, $\rho_t = \rho_0 + t,\ t \in \mathbb{R}$ measures the proportion of the two radii $r_{t,1}$ and $r_{t,2}$ in the transformed motor. Similarly, $x(0)$ describes particles on Γ_0 whereas $x(t)$ stands for the corresponding transformed particles on Γ_t.

For positive values of t, circle 1 enlarges while the second circle reduces its size in equal measure. The amount of increase or reduction is denoted by s.
Figure 3.5 shows the movement of the cog curve for the case $t < 0$. Then, circle 1 gets smaller whereas circle 2 enlarges. The solid circles represent the initial geometry, the dashed ones resulted from changing the ratio ρ. To provide a better imagination, the parts of the circles defining the contour of the cog are colored red. The solid red curve denotes the initial interface Γ_0 between the cog and the coils of wire, the dashed red line denotes Γ_t, the cog curve obtained by variation of ρ. Figure 3.5 also visualizes our chosen transformation T_t, which equals the radial displacement of material particles of length s. Particles $x(0)$ situated on the initial curve Γ_0 are shifted in direction of either the outer normal of a circle or its negative counterpart pointing to the circle center.

To determine the mapping T_t we choose the following ansatz describing the relation between the initial radii, the parameter t and the distance $s(t)$ between initial and transformed particles:

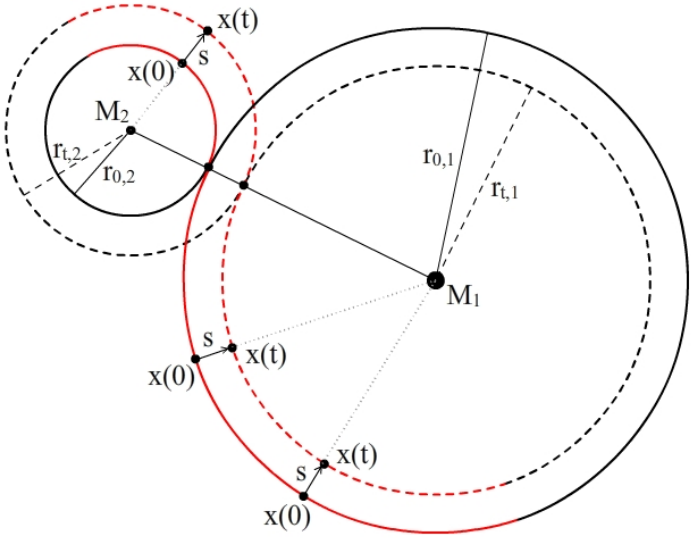

Figure 3.5: Transformation at variation of ratio

Ansatz:

$$\rho_t = \rho_0 + t = \frac{r_{0,1} + s}{r_{0,2} - s} \tag{3.3}$$

Solving for s leads to

$$s(t) = \frac{t\ r_{0,2}}{\rho_0 + t + 1}.$$

Then, the transformation of particles on Γ_0 to their new position on Γ_t is defined by:

$$\begin{aligned} T_t : \Gamma_0 &\rightarrow \Gamma_t \\ x(0) &\rightarrow x(t) = \begin{cases} x(0) + \frac{s(t)}{r_{0,1}}\ \overrightarrow{M_1 x(0)}, & \text{if } x(0) \in \text{circle 1} \\ x(0) - \frac{s(t)}{r_{0,2}}\ \overrightarrow{M_2 x(0)}, & \text{if } x(0) \in \text{circle 2} \end{cases} \end{aligned}$$

Differentiating with respect to t and setting t equal to zero yields the velocity field:

$$\dot{x}(t)\big|_{t=0} = V(0,x) = \begin{cases} \frac{1}{\rho_0(\rho_0+1)} \left(x(0) - M_1\right), & \text{if } x(0) \in \text{circle 1} \\ -\frac{1}{\rho_0+1} \left(x(0) - M_2\right), & \text{if } x(0) \in \text{circle 2} \end{cases}$$

With n denoting the unit outer normal vector of circle 1 and simultaneously the negative unit outer normal of circle 2, i.e.

$$n = \begin{cases} \frac{1}{r_{0,1}} \left(x(0) - M_1 \right), & \text{if } x(0) \in \text{circle 1} \\ -\frac{1}{r_{0,2}} \left(x(0) - M_2 \right), & \text{if } x(0) \in \text{circle 2} \end{cases} \tag{3.4}$$

we obtain

$$v_n(x) = \frac{r_{0,1}}{\rho_0(\rho_0 + 1)} = \frac{r_{0,2}}{\rho_0 + 1}$$

for the normal component of the Eulerian velocity field. Note that v_n is independent on the position on the curve.

3.3.2 Variation of the x-coordinate of M_1

The second design parameter we consider is the x-coordinate of the center of circle 1. Changes in the geometry obtained by its variation are shown in figure 3.6.
Like in figure 3.5, the solid circles denote the initial ones whereas the dashed circles refer to the transformed geometry. Again, the red circular arcs specify the cog curve.

Obviously, $M_{0,1}$ denotes the initial midpoint of circle 1 and $M_{t,1} = M_{0,1} + \binom{t}{0}$ the transformed center after varying the design parameter. Accordingly, for $t > 0$ the center of circle 1 drifts to the right and for $t < 0$ to the left.
As pointed out in figure 3.6, a modification of $x_{M,1}$ leads to a translated midpoint and an alteration in the size of circle 1. Circle 2 also changes its size while the position of M_2 is fixed. Thus, we do not need to introduce further indices for M_2. Both circles either expand or shrink but never change in the opposite direction.
Although in figure 3.6 the two circles are getting bigger for a positive real number t, $t>0$ does not automatically imply increasing circles. Growth or reduction is determined by the sign of t as well as the position of the initial circles to each other.

Figure 3.7 demonstrates how particles $x(0)$ on the original, solid curve are mapped to their corresponding position $x(t)$. The initial and transformed radii of the two circles are denoted like in subsection 3.3.1, the midpoints are named in accordance with figure 3.6.
B_0 and B_t specify the contact points of the circles in the initial and transformed

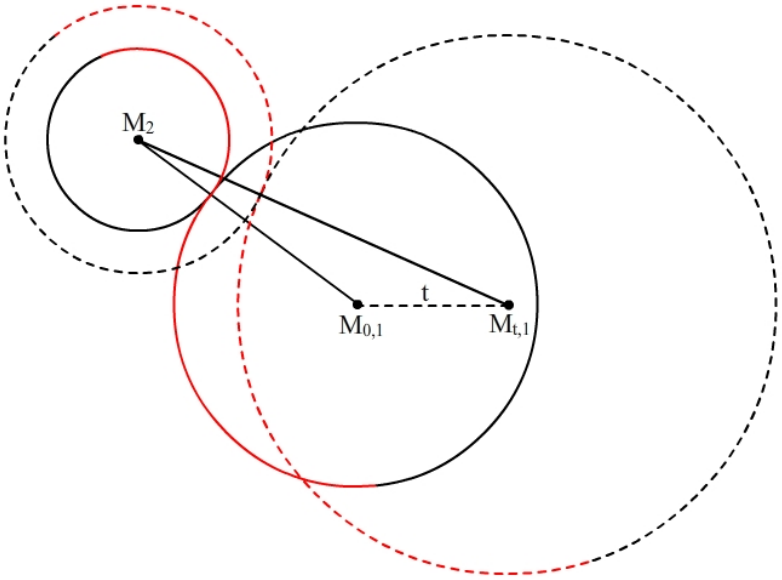

Figure 3.6: Geometrical change at variation of $x_{M,1}$

geometry, repectively. Observe that the line connecting them is parallel to the center-movement, which can be deduced from the *Theorem on intersecting lines*, since the ratio of the radii is constant.
The solid grey circle with the initial midpoint but changed radius of circle 1 is used to describe the mapping T_t. The dotted lines represent artificial lines to visualize how a particle $x(0)$ is transformed, which will be further discussed below.

In the following, a mathematical expression for mapping particles from their original position to the transformed curve is derived.

Preliminary work:

Before we are able to define the map T_t, we have to work out the required preliminaries. First, we will compute the radii $r_{t,1}$ and $r_{t,2}$ of the transformed circles. Then, both the initial and shifted contact points B_0 and B_t of the two circles will be given. The last preparation step that needs to be accomplished is the computation of the sine and cosine of the angle α between $\overrightarrow{M_2B_0}$ and $\overrightarrow{M_2B_t}$.

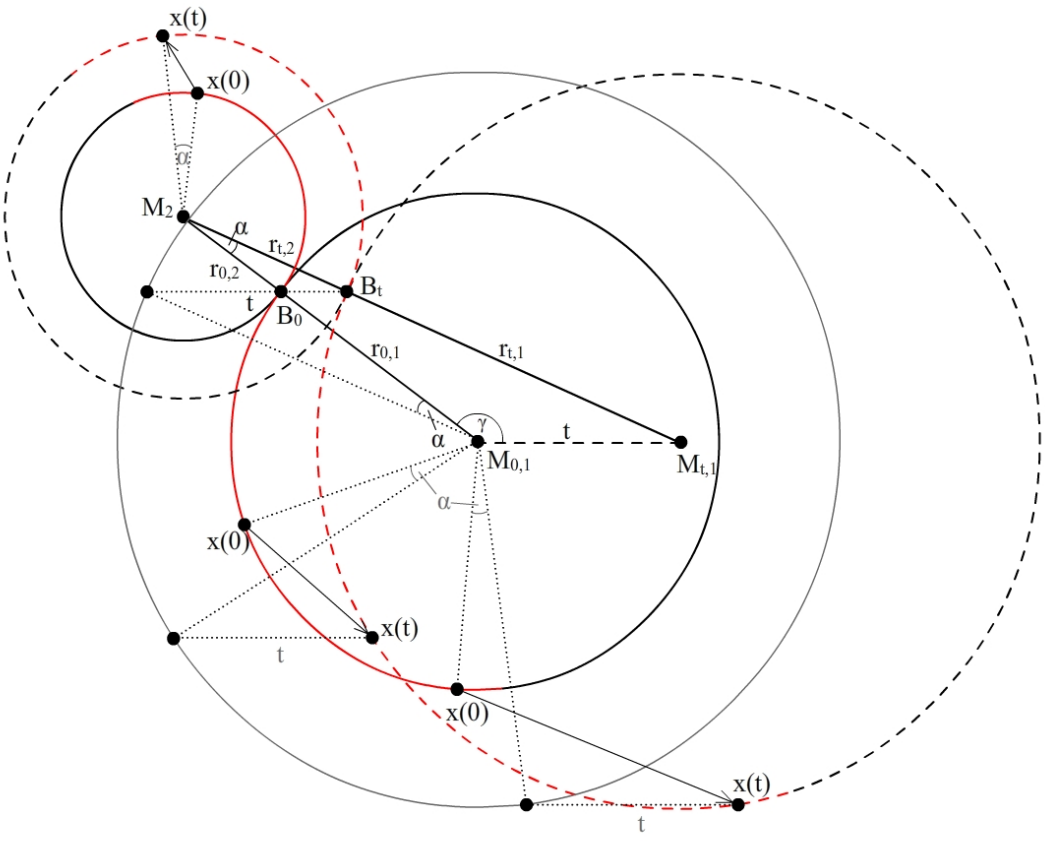

Figure 3.7: Particle displacement at variation of $x_{M,1}$

In order to get a representation of the radii in the transformed geometry in terms of t, the initial ratio ρ_0 and the coordinates of the circle centers, we will state two equations for $r_{t,1}$ and $r_{t,2}$.
On the one hand, the ratio of the two radii is constant which leads to a relation between the two unknowns and the initial ratio. On the other hand, the transformed circles are still tangent. Hence, we claim the distance of their midpoints to equal the sum of the circles' radii, which yields:

$$\text{(I)} \qquad \rho_0 = \rho_t = \frac{r_{t,1}}{r_{t,2}}$$

$$\text{(II)} \qquad r_{t,1} + r_{t,2} = \|\overrightarrow{M_{t,1}M_2}\|.$$

Solving the above system of equations results in

$$r_{t,1} = \frac{\rho_0}{\rho_0+1}\sqrt{(x_2-(x_1+t))^2+(y_2-y_1)^2} = \rho_0\ r_{t,2} \tag{3.5}$$

$$r_{t,2} = \frac{\sqrt{(x_2-(x_1+t))^2+(y_2-y_1)^2}}{\rho_0+1} \tag{3.6}$$

where

$$M_{0,1} = (x_1, y_1), \qquad M_2 = (x_2, y_2).$$

The contact points B_0 and B_t are obtained by simple geometric considerations:

$$\begin{aligned} B_0 &= M_{0,1} + \frac{\rho_0}{\rho_0+1}(M_2 - M_{0,1}) \\ B_t &= M_{t,1} + \frac{\rho_0}{\rho_0+1}(M_2 - M_{t,1}). \end{aligned}$$

Since α describes the angle between $\overrightarrow{M_2B_0}$ and $\overrightarrow{M_2B_t}$, the well-known formula

$$\cos\alpha = \frac{\overrightarrow{M_2B_0}\cdot\overrightarrow{M_2B_t}}{r_{0,2}\ r_{t,2}}$$

with the scalar product $\cdot$ holds. Inserting the known quantities gives

$$\cos\alpha = \frac{1}{r_{0,1}+r_{0,2}}\ \frac{(x_2-x_1)^2 - t(x_2-x_1) + (y_2-y_1)^2}{\sqrt{(x_2-x_1-t)^2+(y_2-y_1)^2}}. \tag{3.7}$$

For the computation of $\sin\alpha$ the *Law of Sines* is applied which leads to the following relation:

$$\sin\alpha = \frac{t\sin\gamma}{r_{t,1}+r_{t,2}} \tag{3.8}$$

where γ denotes the angle between $\overrightarrow{M_{0,1}M_2}$ and the positive x-axis. The sine of γ is given by

$$\sin\gamma = \sqrt{1-(\cos\gamma)^2} \tag{3.9}$$

and

$$\cos\gamma = \frac{\overrightarrow{M_{0,1}M_2}\cdot\binom{1}{0}}{r_{0,1}+r_{0,2}} = \frac{x_2-x_1}{r_{0,1}+r_{0,2}}.$$

Note that $\sin\gamma$ could actually have a negative sign. Since this would imply an angle greater than 180 degrees, which is impossible for our geometrical change, we only consider the positive expression.
Inserting (3.5), (3.6) and (3.9) into (3.8) finally leads to

$$\sin\alpha = \frac{1}{r_{0,1}+r_{0,2}} \frac{t(y_2-y_1)}{\sqrt{(x_2-x_1-t)^2+(y_2-y_1)^2}}. \tag{3.10}$$

Definition of the transformation:

The mapping of particles is dependent on their position on the original curve. More precisely, we distinguish points located on circle 1 and those situated on circle 2.

When the center of circle 1 moves, circle 2 increases or diminishes radially as shown in figure 3.6. Thus, particles on circle 2 are transformed similarly to the case of a varying ratio described in subsection 3.3.1. The difference is that the vector $\overrightarrow{M_2x(0)}$ has to be rotated by α before its length is adjusted to $r_{t,2}$ which ensures that the corresponding particle lies on the transformed curve at the end.

Points belonging to circle 1 are also mapped in a similar way which can be observed in figure 3.6. But now, after rotation of the vector $\overrightarrow{M_1x(0)}$ and adapting its length, the resulting particle additionally needs to be shifted in accordance with the center of circle 1, i.e. it is translated by $\binom{t}{0}$.

Formally, the transformation of particles of the initial curve writes as:

$$T_t : \Gamma_0 \rightarrow \Gamma_t \tag{3.11}$$

$$x(0) \rightarrow x(t) = \begin{cases} \frac{r_{t,1}}{r_{0,1}} R\ \overrightarrow{M_{0,1}x(0)} + M_1 + \binom{t}{0}, & \text{if } x(0) \in \text{circle 1} \\ \frac{r_{t,2}}{r_{0,2}} R\ \overrightarrow{M_2x(0)} + M_2, & \text{if } x(0) \in \text{circle 2} \end{cases} \tag{3.12}$$

with the rotation matrix

$$R = \begin{pmatrix} \cos\alpha & -\sin\alpha \\ \sin\alpha & \cos\alpha \end{pmatrix} \tag{3.13}$$

Computation of v_n:

The Eulerian velocity $V(0,x)$ equates the first derivative of (3.12) with respect to t, evaluated at $t=0$. Using (3.5), (3.6), (3.13), (3.10) and (3.7) yields

$$V(0,x) = \begin{cases} \frac{1}{(r_{0,1}+r_{0,2})^2} \begin{pmatrix} -(x_2-x_1)(x_0-x_1)-(y_2-y_1)(y_0-y_1) \\ (y_2-y_1)(x_0-x_1)-(x_2-x_1)(y_0-y_1) \end{pmatrix} + \begin{pmatrix} 1 \\ 0 \end{pmatrix}, & \text{on circle 1} \\ \frac{1}{(r_{0,1}+r_{0,2})^2} \begin{pmatrix} -(x_2-x_1)(x_0-x_2)-(y_2-y_1)(y_0-y_2) \\ (y_2-y_1)(x_0-x_2)-(x_2-x_1)(y_0-y_2) \end{pmatrix}, & \text{on circle 2} \end{cases}$$

where x_0, y_0 denominate the coordinates of the initial particle $x(0)$.

Let again n denote the unit outer normal vector of circle 1 and the negative unit outer normal of circle 2 as defined in (3.4). The scalar product of $V(0,x)$ and n provides the velocity of the particles on the initial curve in normal direction:

$$v_n(x) = \begin{cases} \frac{-(x_2-x_1)\ r_{0,1}}{(r_{0,1}+r_{0,2})^2} + \frac{x_0-x_1}{r_{0,1}}, & \text{if } x(0) \in \text{circle 1} \\ \frac{-(x_2-x_1)\ r_{0,2}}{(r_{0,1}+r_{0,2})^2}, & \text{if } x(0) \in \text{circle 2} \end{cases} \tag{3.14}$$

Remark 3.3. *Applying the matrix* (3.13) *rotates a vector counterclockwise by an angle α which suffices the case illustrated in figure 3.7. However, the relative position of the three plotted midpoints to each other could as well require a clockwise rotation.*
For example, consider the location of $M_{0,1}$ and M_2 as in figure 3.7 but the case $t<0$ and call the evolving angle α_2. Then, α_2 is greater than 180 degrees, i.e. $\alpha_2 = 360-\alpha$. Rotating counterclockwise by that angle is equivalent to rotate by α in clockwise direction, which corresponds to applying $R^T(\alpha)$ instead of $R(\alpha)$.
The situation described above would lead to some changed signs in both the transformation (3.12) *and the velocity but it would result in the same normal component v_n.*

3.3.3 Summary

For variation of the y-coordinate of M_1 and both coordinates of M_2, the normal components of the velocity fields can be derived analogously to subsection 3.3.2. The results

for v_n are summarized in the following table, where n always denotes the unit outer normal for particles on circle 1 and the unit vector pointing to M_2, if $x(0)$ is located on circle 2:

	$x(0) \in$ circle 1	$x(0) \in$ circle 2
ρ	$r_{0,2}/(\rho_0 + 1)$	$r_{0,2}/(\rho_0 + 1)$
$x_{M,1}$	$-z(x_2 - x_1)r_{0,1} + (x_0 - x_1)/r_{0,1}$	$z(x_2 - x_1)r_{0,2}$
$y_{M,1}$	$-z(y_2 - y_1)r_{0,1} + (y_0 - y_1)/r_{0,1}$	$z(y_2 - y_1)r_{0,2}$
$x_{M,2}$	$z(x_2 - x_1)r_{0,1}$	$-z(x_2 - x_1)r_{0,2} - (x_0 - x_2)/r_{0,2}$
$y_{M,2}$	$z(y_2 - y_1)r_{0,1}$	$-z(y_2 - y_1)r_{0,2} - (y_0 - y_2)/r_{0,2}$

with $z = 1/(r_{0,1} + r_{0,2})^2$, the coordinates (x_0, y_0) of the initial position of a particle, and (x_1, y_1) and (x_2, y_2) the coordinates of the circle midpoints $M_{0,1}$ and $M_{0,2}$, respectively.

Chapter 4

Introduction to Shape Derivatives

Solving the minimization problem (2.1) requires the computation of the gradient of the cost functional with respect to shape variations of Ω. In chapter 5 we will see that this shape gradient depends on u, the solution of the boundary value problem (2.28), as well as on u', the so-called shape derivative of u.
As mentioned before, the latter solves another variational problem on Ω, which can be derived by differentiating the original one for u. Consequently, beside the shape gradient of the cost functional, we are interested in the Eulerian derivatives of both sides of (2.28).
In this chapter we accomplish the preliminary work to compute the Eulerian derivatives needed in chapter 5. In other words, we prepare general differentiation formulas for shape functionals that consist of domain or boundary integrals.

Definition 4.1 (Eulerian derivative)**.** Let $\Omega \subset \mathbb{R}^m$, $J : \Omega \to J(\Omega)$ a functional and let $\Omega_t = T_t(V)(\Omega)$ denote a family of deformations of Ω. The Eulerian derivative of J at Ω in the direction of a vector field V is defined by the limit

$$dJ(\Omega; V) = \lim_{t \downarrow 0} \frac{J(\Omega_t) - J(\Omega)}{t}. \tag{4.1}$$

The Eulerian derivative of the functional J is a directional derivative. It characterizes the behavior of J when Ω moves in the direction of V.

The definition above is given in many books treating shape optimization problems of any kind. For details about the existence of the Eulerian derivative of a functional, shape differentiabilty and needed assumptions on the vector field V, we refer to [15].

The chapter is organized as follows:

The differentiation of domain integrals like those appearing in the boundary value problem for u is covered in section 4.1. Section 4.2 deals with the (more difficult) computation of the Eulerian derivative of boundary integrals. Important differential operators and necessary tools such as the tangential Stokes formula are introduced. Then, we derive a differentiation formula for the type of boundary integral that occurs in the cost functional.

4.1 Domain Integrals

In this section we derive a general formula for the Eulerian derivative of a functional J consisting of an integral over the domain Ω. The integrand F is a function of $x \in \mathbb{R}^2$, a function y of Ω and the gradient of y, i.e.

$$J(\Omega) = \int_\Omega F\big(x, y(\Omega)(x), \nabla y(\Omega)(x)\big)\, d\Omega. \tag{4.2}$$

Remark 4.2. *Note that y is not just a function defined on a part of Ω but depends on the shape of the domain. For instance, y could be the solution of a variational problem on Ω. Consequently, both the integrand and the domain of integration depend on Ω.*

On the transformed domain Ω_t we consider the corresponding functional

$$J(\Omega_t) = \int_{\Omega_t} F\big(x, y(\Omega_t)(x), \nabla y(\Omega_t)(x)\big)\, d\Omega_t. \tag{4.3}$$

Substitution rule and chain rule yield

$$\begin{aligned} J(\Omega_t) &= \int_\Omega F\Big(T_t(x), \left(y(\Omega_t)\circ T_t\right)(x), \left(\nabla y(\Omega_t)\circ T_t\right)(x)\Big)\, \gamma(t)(x)\, d\Omega \\ &= \int_\Omega F\Big(T_t(x), \left(y(\Omega_t)\circ T_t\right)(x), DT_t^{-T}(x)\nabla\left(y(\Omega_t)\circ T_t\right)(x)\Big)\, \gamma(t)(x)\, d\Omega \end{aligned}$$

with the transformation $T_t : \Omega \to \Omega_t$ as in Chapter 3, its Jacobean $DT_t = \left(\frac{\partial T_{t,i}}{\partial x_j} \right)_{i,j=1,2}$ and $\gamma(t) = \det DT_t$. Inserting into (4.1) gives

$$\begin{aligned} dJ(\Omega; V) &= \frac{d}{dt} J(\Omega_t)\Big|_{t=0} \\ &= \frac{d}{dt} \left[\int_\Omega F\Big(T_t(x), \left(y(\Omega_t) \circ T_t\right)(x), DT_t^{-T}(x) \nabla \left(y(\Omega_t) \circ T_t\right)(x) \Big) \ \gamma(t)(x) \ d\Omega \right] \Bigg|_{t=0}. \end{aligned}$$

Since the domain of integration is independent of t, the differential operator $\frac{d}{dt}$ and the integral can be exchanged under the assumption that everything is smooth enough (for details see [15]). Applying product rule and chain rule leads to

$$\begin{aligned} dJ(\Omega; V) &= \int_\Omega F\big(x, y(\Omega)(x), p(\Omega)(x)\big) \ \frac{d}{dt} \gamma(t)(x)\Big|_{t=0} \ d\Omega \\ &\quad + \int_\Omega \Big[D_x F\big(x, y(\Omega)(x), p(\Omega)(x)\big) \ \frac{d}{dt} T_t(x)\Big|_{t=0} \\ &\quad + D_y F\big(x, y(\Omega)(x), p(\Omega)(x)\big) \ \frac{d}{dt} \Big(y(\Omega_t) \circ T_t \Big)(x)\Big|_{t=0} \\ &\quad + D_p F\big(x, y(\Omega)(x), p(\Omega)(x)\big) \ \frac{d}{dt} \Big(DT_t^{-T}(x) \nabla (y(\Omega_t) \circ T_t)(x) \Big)\Big|_{t=0} \Big] \ \gamma(0)(x) \ d\Omega \end{aligned}$$

with the abbreviation $p = \nabla y$. Next we need the following theorem:

Theorem 4.3.

$$\begin{aligned} &\text{(i)} && \det DT_0 = 1 && (4.4) \\ &\text{(ii)} && \frac{d}{dt} DT_t\Big|_{t=0} = DV(0) && (4.5) \\ &\text{(iii)} && \frac{d}{dt} DT_t^T\Big|_{t=0} = DV^T(0) && (4.6) \\ &\text{(iv)} && \frac{d}{dt} DT_t^{-1}\Big|_{t=0} = -DV(0) && (4.7) \\ &\text{(v)} && \frac{d}{dt} DT_t^{-T}\Big|_{t=0} = -DV^T(0) && (4.8) \\ &\text{(vi)} && \frac{d}{dt} \Big(\det DT_t \Big)\Big|_{t=0} = \operatorname{div} V(0) && (4.9) \\ &\text{(vii)} && \frac{d}{dt} \Big(\| DT_t^{-T} n \|_{l_2} \Big)\Big|_{t=0} = -DV(0)n \cdot n && (4.10) \end{aligned}$$

where $\|.\|_{l_2}$ is the Euclidean norm.

Proof. (i) $T_0 = \mathrm{id} \;\Rightarrow\; DT_0 = \mathrm{I} \;\Rightarrow\; \det DT_0 = 1$
(ii) Exchanging the derivatives with respect to x and t (under the assumption that the transformation is smooth enough) and using (3.1) yields

$$\frac{d}{dt} DT_t\Big|_{t=0} = D\Big(\frac{d}{dt} T_t\Big|_{t=0}\Big) = DV(0).$$

(iii) analogous to ii)
(iv) Product rule and ii) lead to

$$\begin{aligned} \frac{d}{dt}\Big(DT_t^{-1}\; DT_t\Big)\Big|_{t=0} &= \frac{d}{dt}\,\mathrm{I}\,\Big|_{t=0} \\ \Leftrightarrow\; \frac{d}{dt} DT_t^{-1}\Big|_{t=0} \underbrace{DT_0}_{=\mathrm{I}} + \underbrace{DT_0^{-1}}_{=\mathrm{I}}\; \frac{d}{dt} DT_t\Big|_{t=0} &= 0 \\ \Leftrightarrow\; \frac{d}{dt} DT_t^{-1}\Big|_{t=0} &= -DV(0). \end{aligned}$$

(v) analogous to iv)
(vi) The first step of the proof requires Jacobi's formula for the derivative of a determinant:

$$\frac{d}{dt}\Big(\det DT_t\Big)\Big|_{t=0} = \mathrm{tr}\Big[\mathrm{adj}(\underbrace{DT_0}_{=\mathrm{I}})\; \frac{d}{dt} DT_t\Big|_{t=0}\Big]$$

where $\mathrm{tr}(A)$ denotes the trace and $\mathrm{adj}(A)$ refers to the adjugate of a matrix A.
Because of $\mathrm{adj}(\mathrm{I}) = \mathrm{I}$ and ii) we have

$$\begin{aligned} \frac{d}{dt}\Big(\det DT_t\Big)\Big|_{t=0} &= \mathrm{tr}\, DV(0) \\ &= \mathrm{div}\, V(0). \end{aligned}$$

(vii) With

$$g(t) := DT_t^{-T} n$$

we get

$$\begin{aligned} \frac{d}{dt}\|g(t)\|_{l_2}\Big|_{t=0} &= \frac{d}{dt}\Big(\sum_i g_i(t)^2\Big)^{\frac{1}{2}}\Big|_{t=0} \\ &= \frac{1}{\|g(0)\|_{l_2}}\Big(g(0)^T\; \frac{d}{dt} g(t)\Big|_{t=0}\Big). \end{aligned}$$

Using $g(0) = n$ it follows $\|g(0)\|_{l_2} = 1$ and

$$\frac{d}{dt} g(t)\Big|_{t=0} = \frac{d}{dt}\Big(DT_t^{-T}\Big)\Big|_{t=0} n \overset{(v)}{=} -DV^T(0)n,$$

and, therefore,

$$\begin{aligned} \frac{d}{dt}\Big(\|DT_t^{-T}n\|_{l_2}\Big)\Big|_{t=0} &= -n^T DV^T(0)n \\ &= -DV(0)n \cdot n. \end{aligned}$$

□

Furthermore, we introduce the material derivative of y as defined in [1] on page 56:

Definition 4.4 (material derivative)**.**

$$\dot{y}(\Omega; V) = \frac{d}{dt}\Big[y(\Omega_t) \circ T_t\Big]\Big|_{t=0} \tag{4.11}$$

The material derivative "characterizes the behavior of y at $x \in \Omega$ in the velocity direction V". (Haslinger/Mäkingen 2003: 111)

Therefore we get, combined with the initial value problem (3.1) and theorem 4.3,

$$\begin{aligned} dJ(\Omega; V) = &\int_\Omega F\big(x, y(\Omega)(x), p(\Omega)(x)\big)\ \operatorname{div} V(0)(x)\ d\Omega \\ &+ \int_\Omega D_x F\big(x, y(\Omega)(x), p(\Omega)(x)\big)\ V(0)(x)\ d\Omega \\ &+ \int_\Omega D_y F\big(x, y(\Omega)(x), p(\Omega)(x)\big)\ \dot{y}(\Omega; V)(x)\ d\Omega \\ &+ \int_\Omega D_p F\big(x, y(\Omega)(x), p(\Omega)(x)\big)\ \Big((\dot{\nabla} y)(\Omega; V)(x) - DV^T(0)(x)\nabla y(\Omega)(x)\Big)\ d\Omega. \end{aligned}$$

From now on we shortly write V for $V(0)(x)$ in this chapter. Assuming that everything is smooth enough, the derivatives with respect to x and t in the material derivative of ∇y can be exchanged, i.e. $(\dot{\nabla} y) = \nabla \dot{y}$. Next we define the so-called shape derivative of y in the direction of V by means of the material derivative:

Definition 4.5 (shape derivative)**.**

$$y'(\Omega;V) = \dot{y}(\Omega;V) - V \cdot \nabla y(\Omega) \tag{4.12}$$

Further details concerning the relation between material derivative and shape derivative can be found in [6] on page 111-112. Then we have

$$\begin{aligned} \nabla\dot{y}(\Omega;V) &= \nabla\Big(y'(\Omega;V) + V \cdot \nabla y(\Omega)\Big) \\ &= \nabla y'(\Omega;V) + DV^T \nabla y(\Omega) + (V \cdot \nabla)\nabla y(\Omega). \end{aligned}$$

Replacing the material derivatives of y by shape derivatives gives

$$\begin{aligned} dJ(\Omega;V) &= \int_\Omega F\big(x, y(\Omega)(x), p(\Omega)(x)\big)\ \operatorname{div} V\ d\Omega \\ &\quad + \int_\Omega D_x F\big(x, y(\Omega)(x), p(\Omega)(x)\big)\ V\ d\Omega \\ &\quad + \int_\Omega D_y F\big(x, y(\Omega)(x), p(\Omega)(x)\big)\ \Big(y'(\Omega;V)(x) + (V \cdot \nabla)y(\Omega)(x)\Big)\ d\Omega \\ &\quad + \int_\Omega D_p F\big(x, y(\Omega)(x), p(\Omega)(x)\big)\ \Big(\nabla y'(\Omega;V)(x) + (V \cdot \nabla)\nabla y(\Omega)(x)\Big)\ d\Omega. \end{aligned}$$

Using the product rule for divergence and applying chain rule we can show the following identity:

$$\begin{aligned} &\operatorname{div}\Big[F\big(x, y(x), p(x)\big)V(x)\Big] \\ &= F\big(x, y(x), p(x)\big)\operatorname{div} V(x) + \nabla\Big[F\big(x, y(x), p(x)\big)\Big] \cdot V(x) \\ &= F\big(x, y(x), p(x)\big)\operatorname{div} V(x) + D_x F\big(x, y(x), p(x)\big)V(x) \\ &\quad + D_y F\big(x, y(x), p(x)\big)D_x y(x)V(x) + D_p F\big(x, y(x), p(x)\big)D_x p(x)V(x) \\ &= F\big(x, y(x), p(x)\big)\operatorname{div} V(x) + D_x F\big(x, y(x), p(x)\big)V(x) \\ &\quad + D_y F\big(x, y(x), p(x)\big)\big(V(x) \cdot \nabla\big)y(x) + D_p F\big(x, y(x), p(x)\big)\big(V(x) \cdot \nabla\big)p(x) \end{aligned}$$

which leads to

$$\begin{aligned} dJ(\Omega;V) &= \int_\Omega D_y F\big(x, y(\Omega)(x), p(\Omega)(x)\big) y'(\Omega;V)(x)\ d\Omega \\ &\quad + \int_\Omega D_p F\big(x, y(\Omega)(x), p(\Omega)(x)\big) \nabla y'(\Omega;V)(x)\ d\Omega \\ &\quad + \int_\Omega \operatorname{div}\Big[F\big(x, y(\Omega)(x), p(\Omega)(x)\big) V\Big]\ d\Omega \end{aligned}$$

or, by using Gauss' theorem,

$$\begin{aligned} dJ(\Omega;V) &= \int_\Omega D_y F\big(x, y(\Omega)(x), p(\Omega)(x)\big) y'(\Omega;V)(x)\ d\Omega \\ &\quad + \int_\Omega D_p F\big(x, y(\Omega)(x), p(\Omega)(x)\big) \nabla y'(\Omega;V)(x)\ d\Omega \\ &\quad + \int_\Gamma F\big(x, y(\Omega)(x), p(\Omega)(x)\big) V \cdot n\ d\Gamma. \end{aligned} \tag{4.13}$$

4.2 Boundary Integrals

4.2.1 Tangential Operators and Formulas

A formal definition of the tangential gradient and tangential divergence can be found in [13], page 13. In our case it is sufficient to introduce the operators on the boundary Γ of Ω by their relation to the corresponding operators in Ω:

Definition 4.6 (Tangential gradient, tangential divergence)**.** Let Γ be the smooth boundary of a domain $\Omega \subset \mathbb{R}^m$ and let the scalar h and the vector V be functions defined on Γ. For given arbitrary extensions $\tilde{h}$ of h and $\tilde{V}$ of V in a neighborhood of Γ, the tangential gradient of h is given by

$$\nabla_\Gamma h = \nabla \tilde{h} - \frac{\partial \tilde{h}}{\partial n}\, n, \tag{4.14}$$

the tangential divergence of V is defined by

$$\operatorname{div}_\Gamma V = \operatorname{div} \tilde{V} - D\tilde{V} n \cdot n, \tag{4.15}$$

where n denotes the surface normal.

The tangential gradient and tangential divergence are independent of the choice of the extensions.

Lemma 4.7. *Tangential gradient and tangential divergence satisfy the counterpart of the product rule for the ordinary divergence:*

$$\operatorname{div}_\Gamma(hV) = \nabla_\Gamma h \cdot V + h \operatorname{div}_\Gamma V. \tag{4.16}$$

Proof. Using the definition of the tangential divergence (4.15) and the common product rule for differentiation yields

$$\begin{aligned} \operatorname{div}_\Gamma(hV) &= \operatorname{div}(\tilde{h}\tilde{V}) - D(\tilde{h}\tilde{V}) n \cdot n \\ &= \tilde{h} \operatorname{div} \tilde{V} + \nabla \tilde{h} \cdot \tilde{V} - \left[\tilde{h} D\tilde{V} + \tilde{V} D\tilde{h} \right] n \cdot n \\ &= \tilde{h} \left[\operatorname{div} \tilde{V} - D\tilde{V} n \cdot n \right] + \left[\nabla \tilde{h} - \frac{\partial \tilde{h}}{\partial n} n \right] \cdot \tilde{V}. \end{aligned}$$

Inserting (4.14) and (4.15) proves the lemma. □

To perform integration by parts on surfaces, we need the following identity:

Theorem 4.8 (Tangential Stokes Formula)**.** *For a differentiable vector valued function w we have*

$$\int_\Gamma \operatorname{div}_\Gamma w \; d\Gamma = \int_\Gamma H \; w \cdot n \; d\Gamma \tag{4.17}$$

with $H = \operatorname{div}_\Gamma n$, the mean curvature of Γ.

4.2.2 Differentiation Formula

Now, a differentiation formula for general boundary integrals, where the integrand F depends on $x \in \mathbb{R}^2$, a function y of the domain Ω enclosed by that boundary, i.e. $\Gamma = \partial\Omega$, and the gradient of y, is provided. We consider

$$J(\Gamma) = \int_\Gamma F\big(x, y(\Omega)(x), \nabla y(\Omega)(x)\big)\, d\Gamma \tag{4.18}$$

and the corresponding functional

$$J(\Gamma_t) = \int_{\Gamma_t} F\big(x, y(\Omega_t)(x), \nabla y(\Omega_t)(x)\big)\, d\Gamma_t \tag{4.19}$$

on the boundary of the transformed domain Ω_t.

After using substitution rule for boundary integrals and applying chain rule to the third argument of F (similarly to section 4.1), we have

$$J(\Gamma_t) = \int_\Gamma F\Big(T_t(x), (y(\Omega_t) \circ T_t)(x), DT_t^{-T}(x)\nabla(y(\Omega_t) \circ T_t)(x)\Big)\, \omega(t)(x)\, d\Gamma \tag{4.20}$$

with

$$\omega(t) = \det DT_t\ \|DT_t^{-T} n\|_{l_2} = \gamma(t)\|DT_t^{-T} n\|_{l_2}. \tag{4.21}$$

From theorem 4.3 directly follows that $\omega(0) = 1$ and

$$\frac{d}{dt}\omega(t)|_{t=0} = \operatorname{div} V(0) - DV(0)n \cdot n = \operatorname{div}_\Gamma V(0).$$

Then, certain smoothness assumptions (for details see [15]) and product rule lead to the following expression for the Eulerian derivative (4.1) of J:

$$
\begin{aligned}
dJ(\Gamma;V) &= \frac{d}{dt}J(\Gamma_t)\Big|_{t=0} \\
&= \int_\Gamma \frac{d}{dt}\Big[F\Big(T_t(x),(y(\Omega_t)\circ T_t)(x),DT_t^{-T}(x)\nabla(y(\Omega_t)\circ T_t)(x)\Big)\ \omega(t)(x)\Big]\Big|_{t=0}\,d\Gamma \\
&= \int_\Gamma F\big(x,y(\Omega)(x),\nabla y(\Omega)(x)\big)\frac{d}{dt}\omega(t)(x)\Big|_{t=0}\,d\Gamma \\
&\quad + \int_\Gamma \frac{d}{dt}F\Big(T_t(x),(y(\Omega_t)\circ T_t)(x),DT_t^{-T}(x)\nabla(y(\Omega_t)\circ T_t)(x)\Big)\Big|_{t=0}\ \omega(0)(x)\ d\Gamma \\
&= \int_\Gamma F\big(x,y(\Omega)(x),\nabla y(\Omega)(x)\big)\,\mathrm{div}_\Gamma V\ d\Gamma \\
&\quad + \int_\Gamma \frac{d}{dt}F\Big(T_t(x),(y(\Omega_t)\circ T_t)(x),DT_t^{-T}(x)\nabla(y(\Omega_t)\circ T_t)(x)\Big)\Big|_{t=0}\,d\Gamma.
\end{aligned}
$$

Following the exact same steps as in section 4.1 (chain rule, product rule, theorem 4.3, inserting material derivatives) yields

$$
\begin{aligned}
dJ(\Gamma;V) &= \int_\Gamma F\big(x,y(\Omega)(x),p(\Omega)(x)\big)\,\mathrm{div}_\Gamma V\ d\Gamma \\
&\quad + \int_\Gamma D_xF\big(x,y(\Omega)(x),p(\Omega)(x)\big)\ V\ d\Gamma \\
&\quad + \int_\Gamma D_yF\big(x,y(\Omega)(x),p(\Omega)(x)\big)\ \dot{y}(\Omega;V)(x)\ d\Gamma \\
&\quad + \int_\Gamma D_pF\big(x,y(\Omega)(x),p(\Omega)(x)\big)\ \Big(\nabla\dot{y}(\Omega;V)(x) - DV^T\nabla y(\Omega)(x)\Big)\ d\Gamma
\end{aligned}
$$

with $p=\nabla y$. For the shape derivative, given by (4.12), we obtain

$$
\begin{aligned}
dJ(\Gamma;V) &= \int_\Gamma F\big(x,y(\Omega)(x),p(\Omega)(x)\big)\,\mathrm{div}_\Gamma V\ d\Gamma \\
&\quad + \int_\Gamma \nabla F\big(x,y(\Omega)(x),p(\Omega)(x)\big)\cdot V\ d\Gamma \\
&\quad + \int_\Gamma D_yF\big(x,y(\Omega)(x),p(\Omega)(x)\big)\ \Big(y'(\Omega;V)(x) + (V\cdot\nabla)y(\Omega)(x)\Big)\ d\Gamma \\
&\quad + \int_\Gamma D_pF\big(x,y(\Omega)(x),p(\Omega)(x)\big)\ \Big(\nabla y'(\Omega;V)(x) + (V\cdot\nabla)\nabla y(\Omega)(x)\Big)\ d\Gamma
\end{aligned}
$$

where we used that $D_xF\ V$ equals $\nabla F\cdot V$.

Now we use relation (4.14) to replace all gradients by tangential gradients:

$$\begin{aligned}
dJ(\Gamma;V) &= \int_\Gamma F\big(x,y(\Omega)(x),p(\Omega)(x)\big)\,\mathrm{div}_\Gamma V\,d\Gamma \\
&\quad+\int_\Gamma \nabla_\Gamma F\big(x,y(\Omega)(x),p(\Omega)(x)\big)\cdot V+\frac{\partial F}{\partial n}\,\big(x,y(\Omega)(x),p(\Omega)(x)\big)\;n\cdot V\;d\Gamma \\
&\quad+\int_\Gamma D_yF\big(x,y(\Omega)(x),p(\Omega)(x)\big)\;\Big(y'(\Omega;V)(x)+V\cdot\frac{\partial y}{\partial n}\,(\Omega)(x)\;n\Big)\;d\Gamma \\
&\quad+\int_\Gamma D_yF\big(x,y(\Omega)(x),p(\Omega)(x)\big)\;V\cdot\nabla_\Gamma y(\Omega)(x)\;d\Gamma \\
&\quad+\int_\Gamma D_pF\big(x,y(\Omega)(x),p(\Omega)(x)\big)\;\Big(\nabla y'(\Omega;V)(x)+\frac{\partial}{\partial n}\big(\nabla y(\Omega)(x)\big)n^T\;V\Big)\;d\Gamma \\
&\quad+\int_\Gamma D_pF\big(x,y(\Omega)(x),p(\Omega)(x)\big)\;\nabla_\Gamma\big(\nabla y(\Omega)(x)\big)\;V\;d\Gamma.
\end{aligned}$$

Since

$$\begin{aligned}
&\mathrm{div}_\Gamma\Big[F\big(x,y(x),p(x)\big)V(x)\Big] \\
&=F\big(x,y(x),p(x)\big)\,\mathrm{div}_\Gamma V(x)+\nabla_\Gamma\Big[F\big(x,y(x),p(x)\big)\Big]\cdot V(x) \\
&=F\big(x,y(x),p(x)\big)\,\mathrm{div}_\Gamma V(x)+\nabla_\Gamma F\big(x,y(x),p(x)\big)\cdot V(x) \\
&\quad+D_yF\big(x,y(x),p(x)\big)\nabla_\Gamma y(x)\cdot V(x)+D_pF\big(x,y(x),p(x)\big)\nabla_\Gamma p(x)V(x)
\end{aligned}$$

the Eulerian derivative equals (with $\dfrac{\partial F}{\partial n}=\nabla F\cdot n$)

$$\begin{aligned}
dJ(\Gamma;V) &= \int_\Gamma \nabla F\big(x,y(\Omega)(x),p(\Omega)(x)\big)\cdot n\;V\cdot n\;d\Gamma \\
&\quad+\int_\Gamma D_yF\big(x,y(\Omega)(x),p(\Omega)(x)\big)\;\Big(y'(\Omega;V)(x)+\frac{\partial y}{\partial n}\,(\Omega)(x)\;V\cdot n\Big)\;d\Gamma \\
&\quad+\int_\Gamma D_pF\big(x,y(\Omega)(x),p(\Omega)(x)\big)\;\Big(\nabla y'(\Omega;V)(x)+\frac{\partial}{\partial n}\big(\nabla y(\Omega)(x)\big)V\cdot n\Big)\;d\Gamma \\
&\quad+\int_\Gamma \mathrm{div}_\Gamma\Big[F\big(x,y(\Omega)(x),p(\Omega)(x)\big)V\Big]\;d\Gamma
\end{aligned}$$

which is, by theorem 4.8, the same as

$$
\begin{aligned}
dJ(\Gamma;V) \;=\; & \int_\Gamma \nabla F\big(x, y(\Omega)(x), p(\Omega)(x)\big)\cdot n\; V\cdot n\; d\Gamma \\
& + \int_\Gamma D_y F\big(x, y(\Omega)(x), p(\Omega)(x)\big)\; \Big(y'(\Omega;V)(x) + \frac{\partial y}{\partial n}\,(\Omega)(x)\; V\cdot n\Big)\; d\Gamma \\
& + \int_\Gamma D_p F\big(x, y(\Omega)(x), p(\Omega)(x)\big)\; \Big(\nabla y'(\Omega;V)(x) + \frac{\partial}{\partial n}\big(\nabla y(\Omega)(x)\big)V\cdot n\Big)\; d\Gamma \\
& + \int_\Gamma HF\big(x, y(\Omega)(x), p(\Omega)(x)\big)V\cdot n\; d\Gamma.
\end{aligned}
\tag{4.22}
$$

with

$$H = \mathrm{div}_\Gamma\, n.$$

Chapter 5

The Main Problem

This chapter deals with the main problem of the thesis. The knowledge gained in the previous chapters is applied to the optimization problem (2.1) given by the ACCM. The first section introduces the cost functional $\mathcal{J}$ and derives a mathematical expression for the function to be minimized. The differentiation formula of subsection 4.2.2 yields the shape gradient of the cost functional.
In section 5.2, the formula for domain integrals and the geometric information worked out in chapter 3 lead to a variational problem for the shape derivative u'.

5.1 The Cost Functional and its Gradient

5.1.1 Specification of the functional

The cost functional originally stated by the ACCM expresses the power of the electric machine in relation to copper losses due to coil resistances, i.e.

$$\mathcal{J} = \frac{3I^2R}{2\omega T} \tag{5.1}$$

with

I	electric current
R	resistance of coils
ω	rotational frequency of rotor (const.)
T	torque.

In this chapter, T stands for torque and is not to be mistaken for the transformation T_t of chapter 3. Note that T refers to the torque computed at a fixed rotor position and not to the average over the torque at different rotor angles.
The main difficulties in (5.1) are associated with the torque since T depends on the geometry of the motor as well as on the state variable u, which again is a function of the domain Ω. The resistance R only has Ω as argument, whereas the remaining variables in (5.1) are constant with respect to both the motor geometry and u. In our model problem we concentrate on T and assume that R is a constant, leading to the following reduced cost functional:

$$\mathcal{J} = \frac{1}{T} \tag{5.2}$$

which still demonstrates the principle idea. This simplified functional describes the power output of the engine ignoring the influence of the occuring copper losses.

5.1.2 Formulation of the cost functional

The torque is given by

$$\vec{T} = \vec{r} \times \vec{F} \tag{5.3}$$

with the force $\vec{F}$ and the lever arm vector $\vec{r}$.

To describe the force affecting a body in a magnetic field and thus the resulting torque, we introduce the Maxwell stress tensor as defined in [11], page 14:

$$\vec{\vec{\sigma}} = \mu \begin{pmatrix} H_1^2 - \frac{1}{2}H^2 & H_1H_2 & H_1H_3 \\ H_2H_1 & H_2^2 - \frac{1}{2}H^2 & H_2H_3 \\ H_3H_1 & H_3H_2 & H_3^2 - \frac{1}{2}H^2 \end{pmatrix} \tag{5.4}$$

with the magnetic field strength $\mathbf{H}$, its magnitude H and the magnetic permeability μ. Using (5.4) and Gauss Theorem, the force acting on a body B writes as

$$\begin{aligned} \vec{F} &= \int_B \operatorname{div} \vec{\vec{\sigma}} \, d\vec{x} \\ &= \int_{\partial B} \vec{\vec{\sigma}} \cdot n \, ds, \end{aligned} \tag{5.5}$$

where n denotes the unit outer normal on the surface of B. Hence, the magnetic field at the surface of B yields the force acting on the body.

In the given problem, we are interested in the effect of the force acting on the rotor. Therefore, we consider the intersection of B in the x_1x_2-plane, which describes a circular disk with the center positioned in the origin. Its boundary is denoted by Γ_0. For numerical reasons, the integration curve in (5.5) is extended from the rotor boundary Γ_0 to a circle defining the outer boundary of the air gap, which can be done without any problems. In the following, Γ_0 denotes the extended integration curve.
Since the x_3-axis describes the rotation axis, the torque vector $\vec{T}$ points in the direction of the x_3-axis and the magnitude equals the third component T_3. From now on, T_3 is referred to as torque and shortly denoted by T.

From (5.3), (5.5), the definition of the symmetric stress tensor (5.4), the constitutive law (2.6), the relation (2.18) and $n = \frac{1}{\sqrt{x_1^2+x_2^2}}\binom{x_1}{x_2}$ we obtain the following expression for the torque:

$$\begin{aligned} T &= \frac{1}{\mu_0}\int_{\Gamma_0} \frac{1}{\sqrt{x_1^2+x_2^2}}\left[\left(\left(\frac{\partial u}{\partial x_1}\right)^2 - \left(\frac{\partial u}{\partial x_2}\right)^2\right)x_1x_2 - \frac{\partial u}{\partial x_1}\frac{\partial u}{\partial x_2}\left(x_1^2-x_2^2\right)\right] d\Gamma_0 \\ &= \frac{1}{\mu_0}\int_{\Gamma_0} \nabla u(\Omega)(x)^T Q(x) \nabla u(\Omega)(x)\, d\Gamma_0 \end{aligned} \tag{5.6}$$

with the symmetric matrix

$$Q(x) = \frac{1}{\sqrt{x_1^2+x_2^2}}\begin{pmatrix} x_1x_2 & \frac{x_2^2-x_1^2}{2} \\ \frac{x_2^2-x_1^2}{2} & -x_1x_2 \end{pmatrix}, \tag{5.7}$$

the curve Γ_0 describing the outer boundary of the air gap and the domain Ω denoting the motor.
Inserting T into (5.2) yields the final expression of the cost functional $\mathcal{J}$.

5.1.3 Computation of the gradient

This subsection deals with the differentiation of the cost functional (5.2) with T given in (5.6) with respect to the geometry of the motor. Obviously, the computation of $dT(\Gamma_0; V)$ is sufficient to determine the shape gradient of $\mathcal{J}$, by quotient rule.

Because T represents a functional consisting of a boundary integral, the type of formulas derived in section 4.2 are applicable.

Remark 5.1. *So far, we have discussed Eulerian derivatives of functionals J, denoted by $dJ(\Omega; V)$ (or $dJ(\Gamma; V)$). This quantity describes the derivative of J at the movement of Ω (or Γ) in direction of the velocity field V, which evolves from variation of one design parameter t. Hence, dJ is the partial derivative of J with respect to a certain design parameter.*
The shape gradient of the cost functional defines a vector collecting the Eulerian derivatives for each considered design parameter. It will be denominated by $D\mathcal{J}$ throughout the thesis.

Let F be the integrand of T, i.e.

$$F(x, u, p) = p^T Q(x) p.$$

Then, for the torque we obtain

$$T(\Gamma_0) = \frac{1}{\mu_0} \int_{\Gamma_0} F(x, u(\Omega)(x), \nabla u(\Omega)(x)) \, d\Gamma_0. \tag{5.8}$$

Applying the differentiation formula (4.22) from subsection 4.2.2 yields

$$\begin{aligned} dT(\Gamma_0; V) \;=\; & \frac{1}{\mu_0} \Bigg[\int_{\Gamma_0} \nabla F\big(x, u(\Omega)(x), \nabla u(\Omega)(x)\big) \cdot n \; v_n \; d\Gamma_0 \\ & + \int_{\Gamma_0} D_u F\big(x, u(\Omega)(x), \nabla u(\Omega)(x)\big) \; \Big(u'(\Omega; V)(x) + \frac{\partial u}{\partial n} \, (\Omega)(x) \; v_n \Big) \; d\Gamma_0 \\ & + \int_{\Gamma_0} D_p F\big(x, u(\Omega)(x), \nabla u(\Omega)(x)\big) \; \Big(\nabla u'(\Omega; V)(x) + \frac{\partial}{\partial n} \big(\nabla u(\Omega)(x) \big) v_n \Big) \; d\Gamma_0 \\ & + \int_{\Gamma_0} HF\big(x, u(\Omega)(x), \nabla u(\Omega)(x)\big) v_n \; d\Gamma_0 \Bigg] \end{aligned}$$

with H denoting the mean curvature of Γ_0 and $v_n = V \cdot n$ referring to the normal component of the velocity V discussed in chapter 3.

Since we determine the optimal shape of the cogs whereas all other parts of the motor remain unchanged, the integration curve Γ_0 is constant with respect to t. Hence v_n,

describing the velocity of particles on Γ_0 in normal direction due to variation of design parameters, equals zero.
With $D_u F = 0$ and $D_p F = 2Qp$, we can finally state the derivative of T with respect to the geometry:

$$dT(\Gamma_0; V) = \frac{2}{\mu_0} \int_{\Gamma_0} Q(x) \nabla u(\Omega)(x) \cdot \nabla u'(\Omega; V)(x) \; d\Gamma_0. \tag{5.9}$$

5.2 Differentiation of the Variational Problem

Equation (5.9) points out the dependence of the gradient of the cost functional on the state variable u and its shape derivative u'. As mentioned earlier, $u(\Omega)$ is given as the solution of the boundary value problem (2.28), whereas $u'(\Omega; V)$ solves the variational problem obtained by differentiating the existing one. In this section we compute the derivatives of both sides of (2.28) using the technique explained in the previous chapter. First, we concentrate on the case of only one material, i.e. one domain Ω with boundary $\Gamma = \partial\Omega$.

We start considering the corresponding variational problem on the transformed domain $\Omega_t = T_t(\Omega)$ with solution $u_t = u(\Omega_t)$:

$$a_t(u_t, v_t) = \langle f_t, v_t \rangle \qquad \forall v_t = v(\Omega_t) \in V(\Omega_t) = \{ v \circ T_t^{-1} : v \in V(\Omega) = H_0^1(\Omega) \} \tag{5.10}$$

with

$$a_t(u_t, v_t) = \int_{\Omega_t} q(\nabla u(\Omega_t))(x) \cdot \nabla v(\Omega_t)(x) \; d\Omega_t \qquad \text{and} \tag{5.11}$$

$$\langle f_t, v_t \rangle = \int_{\Omega_t} \Big(J_3(\Omega_t)(x) v(\Omega_t)(x) + M_\perp(\Omega_t)(x) \cdot \nabla v(\Omega_t)(x) \Big) \; d\Omega_t. \tag{5.12}$$

Below we concentrate on the differentiation of the left-hand side $a(u, v)$. For the sake of clarity we quit writing the dependence of all quantities on x. We define

$$F(x, y, p) = q(p_1) \cdot p_2. \tag{5.13}$$

Then, the left-hand sides of (2.28) and the transformed problem (5.10) have the following form:

$$a(u,v) = \int_\Omega F(x, y(\Omega), p(\Omega))\ d\Omega \tag{5.14}$$

$$a_t(u_t,v_t) = \int_{\Omega_t} F(x, y(\Omega_t), p(\Omega_t))\ d\Omega_t \tag{5.15}$$

with

$$y = \begin{bmatrix} u \\ v \end{bmatrix} \qquad \text{and} \qquad p = \begin{bmatrix} \nabla u \\ \nabla v \end{bmatrix}. \tag{5.16}$$

Applying (4.13), the differentiation formula for functionals consisting of domain integrals, gives

$$\begin{aligned} da(u,v) = & \int_\Omega \Big(D_{y_1} F(x, y(\Omega), p(\Omega))\ u'(\Omega;V) + D_{y_2} F(x, y(\Omega), p(\Omega))\ v'(\Omega;V) \Big)\ d\Omega \\ & + \int_\Omega \Big(D_{p_1} F(x, y(\Omega), p(\Omega))\ \nabla u'(\Omega;V) + D_{p_2} F(x, y(\Omega), p(\Omega))\ \nabla v'(\Omega;V) \Big)\ d\Omega \\ & + \int_\Gamma F(x, y(\Omega), p(\Omega))\ v_n\ d\Gamma. \end{aligned}$$

Because of $v_t = v \circ T_t^{-1}$, it directly follows from the definition of material derivatives, definition 4.4, that

$$\dot{v}(\Omega;V) = 0$$

which leads, with relation (4.12) between shape and material derivatives, to

$$v'(\Omega;V) = -V \cdot \nabla v(\Omega). \tag{5.17}$$

Then, inserting $D_{y_1}F = D_{y_2}F = 0$, $D_{p_1}F = Dq(p_1)p_2$ and $D_{p_2}F = q(p_2)$ and applying integration by parts yields

$$\begin{aligned} da(u,v) &= \int_\Omega \Big(Dq(\nabla u(\Omega))\nabla u'(\Omega;V)\cdot\nabla v(\Omega) + q(\nabla u(\Omega))\cdot\nabla v'(\Omega;V)\Big)\, d\Omega \\ &\quad + \int_\Gamma q(\nabla u(\Omega))\cdot\nabla v(\Omega)\; v_n \; d\Gamma \\ &= \int_\Omega \Big(Dq(\nabla u(\Omega))\nabla u'(\Omega;V)\cdot\nabla v(\Omega) - q(\nabla u(\Omega))\cdot\nabla\left(V\cdot\nabla v(\Omega)\right)\Big)\, d\Omega \\ &\quad + \int_\Gamma q(\nabla u(\Omega))\cdot\nabla v(\Omega)\; v_n \; d\Gamma \\ &= \int_\Omega \Big(Dq(\nabla u(\Omega))\nabla u'(\Omega;V)\cdot\nabla v(\Omega) + \operatorname{div} q(\nabla u(\Omega))V\cdot\nabla v(\Omega)\Big)\, d\Omega \\ &\quad + \int_\Gamma \Big(q(\nabla u(\Omega))\cdot\nabla v(\Omega)\; v_n - V\cdot\nabla v(\Omega)\; q(\nabla u(\Omega))\cdot n\Big)\, d\Gamma \end{aligned}$$

with

$$Dq(p) = \begin{cases} \nu(|p|)\,\mathrm{I} + \frac{\nu'(|p|)}{|p|} pp^T, & \text{if } p \neq 0 \\ \nu(|p|)\,\mathrm{I}, & \text{if } p = 0 \end{cases} \tag{5.18}$$

and the identity matrix I.

Next, we pay attention to the right-hand side of the variational problem (2.28) and define

$$F(x,y,p) = y_1 y_2 + y_3 \cdot p_2. \tag{5.19}$$

Using

$$\begin{array}{lll} D_{y_1}F = y_2 & D_{y_2}F = y_1 & D_{y_3}F = p_2^T \\ D_{p_1}F = 0 & D_{p_2}F = y_3^T & D_{p_3}F = 0 \end{array}$$

with

$$y = \begin{bmatrix} J_3 \\ v \\ M_\perp \end{bmatrix}, \qquad p = \begin{bmatrix} \nabla J_3 \\ \nabla v \\ \nabla M_\perp \end{bmatrix} \tag{5.20}$$

and applying the same steps as before yields

$$\begin{aligned}
d\langle f, v\rangle &= \int_\Omega \Big(J_3'(\Omega;V)v(\Omega) + J_3(\Omega)v'(\Omega;V) + M_\perp'(\Omega;V)\cdot\nabla v(\Omega)\Big)\, d\Omega \\
&\quad + \int_\Omega M_\perp(\Omega)\cdot\nabla v'(\Omega;V)\, d\Omega + \int_\Gamma \Big(J_3(\Omega)v(\Omega) + M_\perp(\Omega)\cdot\nabla v(\Omega)\Big)\, v_n\, d\Gamma \\
&= \int_\Omega \Big(J_3'(\Omega;V)v(\Omega) - J_3(\Omega)V\cdot\nabla v(\Omega) + M_\perp'(\Omega;V)\cdot\nabla v(\Omega)\Big)\, d\Omega \\
&\quad - \int_\Omega M_\perp(\Omega)\cdot\nabla\left(V\cdot\nabla v(\Omega)\right)\, d\Omega + \int_\Gamma \Big(J_3(\Omega)v(\Omega) + M_\perp(\Omega)\cdot\nabla v(\Omega)\Big)\, v_n\, d\Gamma \\
&= \int_\Omega \Big(J_3'(\Omega;V)v(\Omega) - J_3(\Omega)V\cdot\nabla v(\Omega) + M_\perp'(\Omega;V)\cdot\nabla v(\Omega)\Big)\, d\Omega \\
&\quad + \int_\Omega \operatorname{div} M_\perp(\Omega)V\cdot\nabla v(\Omega)\, d\Omega - \int_\Gamma V\cdot\nabla v(\Omega)\; M_\perp(\Omega)\cdot n\, d\Gamma \\
&\quad + \int_\Gamma \Big(J_3(\Omega)v(\Omega) + M_\perp(\Omega)\cdot\nabla v(\Omega)\Big)\, v_n\, d\Gamma.
\end{aligned}$$

Putting both sides together and taking the classical formulation of the boundary value problem for u:

$$-\operatorname{div} q(\nabla u(\Omega)) = J_3(\Omega) - \operatorname{div} M_\perp(\Omega) \qquad \text{in } \Omega$$

into account gives the following expression:

$$\begin{aligned}
\int_\Omega \Big(Dq(\nabla u(\Omega))\nabla u'(\Omega;V)\cdot\nabla v(\Omega)\Big)\, d\Omega &= \int_\Omega \Big(J_3'(\Omega;V)v(\Omega) + M_\perp'(\Omega;V)\cdot\nabla v(\Omega)\Big)\, d\Omega \\
+ \int_\Gamma J_3(\Omega)v(\Omega)\; v_n\, d\Gamma + \int_\Gamma \Big(M_\perp(\Omega) - q(\nabla u(\Omega))\Big)\cdot\nabla v(\Omega)\; v_n\, d\Gamma & \qquad (5.21) \\
+ \int_\Gamma \Big(q(\nabla u(\Omega)) - M_\perp(\Omega)\Big)\cdot n\; V\cdot\nabla v(\Omega)\, d\Gamma.
\end{aligned}$$

The integrals over Γ in (5.21) vanish because of $v_n = 0$ and the following identities obtained by (4.14), theorem 4.8 and considering boundary condition (2.26):

$$\begin{aligned}
&\int_\Gamma \Big(q(\nabla u(\Omega)) - M_\perp(\Omega)\Big)\cdot n\; V\cdot\nabla v(\Omega)\, d\Gamma \\
&= \int_\Gamma \Big(q(\nabla u(\Omega)) - M_\perp(\Omega)\Big)\cdot n\; V\cdot\Big(\nabla_\Gamma v(\Omega) + n\,\frac{\partial v}{\partial n}\,(\Omega)\Big)\, d\Gamma \\
&= -\int_\Gamma \operatorname{div}_\Gamma\Big([q(\nabla u(\Omega)) - M_\perp(\Omega)]\cdot n\; V\Big) v(\Omega)\, d\Gamma + \int_\Gamma Hv(\Omega)V\cdot n\, d\Gamma \\
&= 0.
\end{aligned}$$

Thus, for the case of one domain Ω and Dirichlet boundary conditions we get the following boundary value problem for the shape derivative u':

$$\int_\Omega \Big(Dq(\nabla u(\Omega))\nabla u'(\Omega;V)\cdot\nabla v(\Omega)\Big)\ d\Omega \ = \int_\Omega \Big(J_3'(\Omega;V)v(\Omega) + M_\perp'(\Omega;V)\cdot\nabla v(\Omega)\Big)\ d\Omega$$

with Dq defined in (5.18). From now on, we neglect the dependency of the quantities on Ω and V.

In the following, let Ω be a domain that consists of several subdomains $\Omega^{(i)}$ with boundaries $\partial\Omega^{(i)}$, as defined in section 2.4. Then, (5.21) writes as

$$\begin{aligned}\sum_i \int_{\Omega^{(i)}} \Big(Dq_i(\nabla u_i)\nabla u_i'\cdot\nabla v\Big)\ dx &= \sum_i \int_{\Omega^{(i)}} \Big(J_3^{(i)\prime} v + M_\perp^{(i)\prime}\cdot\nabla v\Big)\ dx \\ &+ \sum_i \int_{\partial\Omega^{(i)}} J_3^{(i)} v\ v_n^{(i)}\ ds + \sum_i \int_{\partial\Omega^{(i)}} \Big(M_\perp^{(i)} - q_i(\nabla u_i)\Big)\cdot\nabla v\ v_n^{(i)}\ ds \\ &+ \sum_i \int_{\partial\Omega^{(i)}} \Big(q_i(\nabla u_i) - M_\perp^{(i)}\Big)\cdot n^{(i)}\ V\cdot\nabla v\ ds\end{aligned}$$

with $v_n^{(i)} = V\cdot n^{(i)}$, where $n^{(i)}$ denotes the unit outer normal to $\Omega^{(i)}$ and with u_i and $J_3^{(i)}$ denoting the restrictions of u and J_3 to $\Omega^{(i)}$. By use of the jump notation introduced on page 12, we obtain

$$\begin{aligned}\sum_i \int_{\Omega^{(i)}} \Big(Dq_i(\nabla u_i)\nabla u_i'\cdot\nabla v\Big)\ dx &= \sum_i \int_{\Omega^{(i)}} \Big(J_3^{(i)\prime} v + M_\perp^{(i)\prime}\cdot\nabla v\Big)\ dx \\ &+ \sum_{\substack{i,j\\ i<j}} \int_{\Gamma^{(i,j)}} \Big[J_3 v\ v_n\Big]\ ds + \sum_{\substack{i,j\\ i<j}} \int_{\Gamma^{(i,j)}} \Big[\Big(M_\perp - q(\nabla u)\Big) v_n\Big]\cdot\nabla v\ ds \\ &+ \sum_{\substack{i,j\\ i<j}} \int_{\Gamma^{(i,j)}} \Big[\Big(q(\nabla u) - M_\perp\Big)\cdot n\Big]\ V\cdot\nabla v\ ds.\end{aligned} \tag{5.22}$$

Note that all integrals over the outer boundary Γ vanish analogously to the case of one domain Ω. From the interface condition (2.25) we immediately get:

$$\int_{\Gamma^{(i,j)}} \Big[\Big(q(\nabla u) - M_\perp\Big)\cdot n\Big]\ V\cdot\nabla v\ ds = 0$$

for all interfaces $\Gamma^{(i,j)}$.

Moreover, the current density J_3 is a constant in each subdomain of the given motor and hence $\nabla J_3 = 0$. For the material derivative (4.11) we get

$$\dot{J}_3(\Omega; V) = \lim_{t \downarrow 0} \frac{1}{t}\Big(J_3(\Omega_t) \circ T_t - J_3(\Omega)\Big) = \lim_{t \downarrow 0} \frac{1}{t}\Big(J_3 - J_3\Big) = 0 \qquad \text{in } \Omega$$

which implies

$$J_3'(\Omega; V) = 0 \qquad \text{in } \Omega.$$

The permanent magnetization $M_\perp$ occurs only in the rotor. When considering geometrical changes regarding the shape of the cogs which does not affect the design of the rotor, the derivative of $M_\perp$ with respect to the geometry, $M_\perp'$, equals zero everywhere in Ω.

With these simplifications, (5.22) can be reduced to

$$\begin{aligned} \sum_i \int_{\Omega^{(i)}} \Big(Dq_i(\nabla u_i)\nabla u_i' \cdot \nabla v\Big)\, dx \;=\; \\ \sum_{\substack{i,j \\ i<j}} \int_{\Gamma^{(i,j)}} \Big[J_3 v\; v_n\Big]\, ds + \sum_{\substack{i,j \\ i<j}} \int_{\Gamma^{(i,j)}} \Big[\Big(M_\perp - q(\nabla u)\Big)v_n\Big] \cdot \nabla v\; ds. \end{aligned} \tag{5.23}$$

Observe that, contrary to the original problem for u, the derived boundary value problem for u' is linear.

Actually we could stop at this point and use the above formulation of the variational problem for u' for a finite element discretization. However, the functional expressing the right-hand side of (5.23) is not well-defined in $H^1(\Omega)$ because of the occurence of $q(\nabla u) \cdot \nabla v$ on the interfaces. Hence, the existence of a unique solution cannot be guaranteed by the *Lax-Milgram Theorem* and furthermore, *Cea's Theorem* is not applicable for estimating the discretization error. If we still discretize equation (5.23) and then compute a solution, we obtain wrong approximate values for the shape derivative u', as we will see for a simple test example in section 6.1.

In the following we will show that in our model problem, the term that causes the numerical problems:

$$\int_{\Gamma^{(i,j)}} \Big(M_{\perp}^{(i)} - q_i(\nabla u_i) \Big) \cdot \nabla v \; v_n^{(i)} \; ds \tag{5.24}$$

can be eliminated, but therefore we have to go back to (5.22) and consider the term

$$\int_{\Gamma^{(i,j)}} \Big(\Big[\Phi(\nabla u) \cdot n \Big] V \cdot \nabla v - \Big[\Phi(\nabla u) \; v_n \Big] \cdot \nabla v \Big) \; ds \tag{5.25}$$

with

$$\Phi(\nabla u) = q(\nabla u) - M_{\perp}.$$

The inner product of ∇v and a vector whose normal component vanishes is equal to the scalar product of the tangential gradient $\nabla_\Gamma v$ and this vector, i.e. $z \cdot \nabla v = z \cdot \nabla_\Gamma v$, if $z \cdot n = 0$. By rewriting (5.25) as

$$\int_{\Gamma^{(i,j)}} \Big(\Big[\Phi(\nabla u) \cdot n \Big] V - \Big[v_n \; \Phi(\nabla u) \Big] \Big) \cdot \nabla v \; ds,$$

it is easy to see that the first term of the inner product has no normal component leading to

$$\int_{\Gamma^{(i,j)}} \Big(\Big[\Phi(\nabla u) \cdot n \Big] V - \Big[v_n \; \Phi(\nabla u) \Big] \Big) \cdot \nabla_\Gamma v \; ds,$$

which, by interface condition and (2.25) and the same argument as before, can be further transformed to

$$\begin{aligned} & - \int_{\Gamma^{(i,j)}} \Big[v_n \; \Phi(\nabla u) \Big] \cdot \nabla_\Gamma v \; ds \\ = \; & - \int_{\Gamma^{(i,j)}} \Big[v_n \; \Big(\nu(|\nabla u|) \nabla u - M_{\perp} \Big) \Big] \cdot \nabla_\Gamma v \; ds \\ = \; & - \int_{\Gamma^{(i,j)}} \Big[v_n \; \Big(\nu(|\nabla u|) \nabla_\Gamma u - M_{\perp} \Big) \Big] \cdot \nabla_\Gamma v \; ds. \end{aligned} \tag{5.26}$$

Contrary to ∇u and ∇v on $\Gamma^{(i,j)}$ in (5.23), the tangential gradients of u and v are well-defined in $H^1(\Omega)$. In our model problem we only consider linear materials, i.e. piecewise constant ν, and assume that ν and $M_\perp$ do not have a jump at the interfaces that are moved to find the optimal geometry of the motor. Then, the jump term in (5.26) equals

zero.
Note that on fixed interfaces (5.26) and also the troublesome term (5.24) vanish immediately because of $v_n = 0$, which leads to the final boundary value problem for the shape derivative u':

$$\sum_i \int_{\Omega^{(i)}} \Big(Dq_i(\nabla u_i)\nabla u_i' \cdot \nabla v \Big)\, dx = \sum_{\substack{i,j \\ i<j}} \int_{\Gamma^{(i,j)}} \Big[J_3 v\ v_n \Big]\, ds. \tag{5.27}$$

Now we have everything needed to solve the given optimization problem:
A mathematical expression of the cost functional $\mathcal{J}$ characterizing the torque of an electric machine was derived in section 5.1. The state variable u appearing in that functional is given as the solution of the boundary value problem (2.28) derived in chapter 2.
The shape gradient of the cost functional was computed in subsection 5.1.3. Moreover the shape derivative u', occuring in $d\mathcal{J}$ besides u, is available by solving the linear variational problem derived above.
The quantity v_n denotes the normal component of the Eulerian velocity. In chapter 3 we computed for variation of each design parameter the corresponding v_n. Thus, we have five boundary value problems leading to five distinct shape derivatives u'. Inserting each individual u' into $d\mathcal{J}$ represents the partial derivatives of $\mathcal{J}$ and therefore yields the shape gradient $D\mathcal{J}$ of the cost functional.

Chapter 6

Numerical Results

For all numerical computations in this chapter we use the simulation program ParNFB, a parallel solver for nonlinear coupled FEM/BEM (boundary element method) systems, developed by Dr. Clemens Pechstein at the Institute of Computational Mathematics at JKU Linz.
The user identifies the design parameter to be considered and inputs its value. Then, ParNFB generates for this geometry a finite element mesh of the motor and solves both the nonlinear BVP for u and the linear problem for the shape derivative u', i.e. it computes the values of the two quantities in all mesh nodes.
Moreover, it returns the function values of the cost functional $\mathcal{J}$ and its Eulerian derivative $d\mathcal{J}$ with respect to shape changes due to the chosen design parameter. Collecting the simulations for all parameters yields the shape gradient $D\mathcal{J}$ of the cost functional. Since we consider in both the test and the original problem only one design parameter, the program output for the derivative already equals the shape gradient.

6.1 Simplified Test Problem

Before we discuss the numerical results of the given problem, we introduce a simple test problem with a known analytic solution. For this example, we will compute the exact solution u, the shape derivative u' and the exact values of a cost functional and its shape gradient. Then we compare these calculations with the numerical computations to verify the programming code.

6.1.1 Problem Description

We consider a rotationally symmetric domain Ω consisting of two subdomains $\Omega^{(1)}$ and $\Omega^{(2)}$ as visualized in figure 6.1. The material data is simplified in such a way that the resulting problem is linear. The magnetic permeability μ is constantly set to 1 on the whole domain and we neglect the permanent magnetization $M_\perp$ in $\Omega^{(1)}$. Moreover, the current density J_3 vanishes in $\Omega^{(1)}$, whereas we define $J_3 = 1$ in $\Omega^{(2)}$, i.e. we specify a jump of the current density on the interface $\Gamma^{(1,2)}$.
We treat geometric changes of Ω obtained by varying the radius R of the inner circle, which means that $\Gamma^{(1,2)}$ expands or shrinks radially.

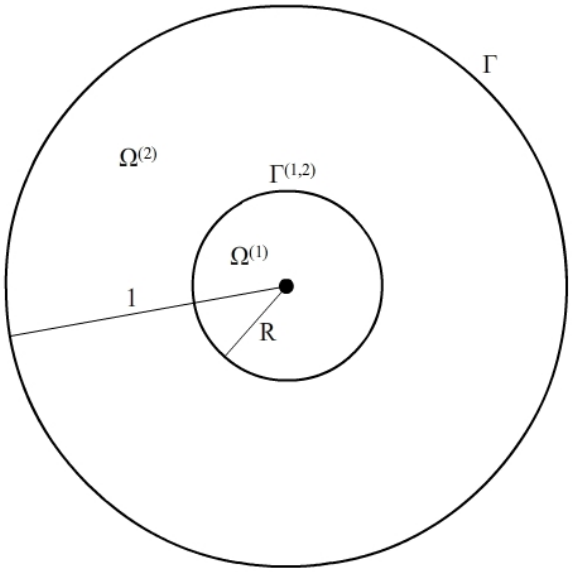

Figure 6.1: Domain for the test problem

6.1.2 Boundary value problem for u

Classical Formulation:

With the setting above we obtain from the classical formulation (2.23)-(2.26) the following boundary value problem for u: Find $u : \bar{\Omega} \rightarrow \mathbb{R}$ such that

$$
\begin{aligned}
-\Delta u &= k, \qquad k = \begin{cases} 0, & \text{in } \Omega^{(1)} \\ 1, & \text{in } \Omega^{(2)} \end{cases} && (6.1)\\
u_1 &= u_2 \qquad \text{on } \Gamma^{(1,2)} && (6.2)\\
\left[\frac{\partial u}{\partial n}\right] &= 0 \qquad \text{on } \Gamma^{(1,2)} && (6.3)\\
u &= 0 \qquad \text{on } \Gamma && (6.4)
\end{aligned}
$$

which can be transformed into a BVP of a second order ordinary differential equation:

$$
\begin{aligned}
-\frac{\partial^2 u}{\partial r^2}(r) - \frac{1}{r}\frac{\partial u}{\partial r}(r) &= k, \qquad k = \begin{cases} 0, & 0 \le r < R \\ 1, & R < r < 1 \end{cases} && (6.5)\\
u_1(R) &= u_2(R) && (6.6)\\
\left[\frac{\partial u}{\partial n}(R)\right] &= 0 && (6.7)\\
u(1) &= 0 && (6.8)
\end{aligned}
$$

with $r = \sqrt{x_1^2 + x_2^2}$.

Exact solution u_e:

The theory of ordinary differential equations (reduction to first order, separation of variables to solve the homogeneous equation, deducing the inhomogeneous solution by variation of the constant) and prescribing the given interface and boundary conditions (6.6)-(6.8) yields the exact solution

$$
u_e(r) = \begin{cases} \frac{1}{4}(1 - R^2) + \frac{R^2}{2}\ln R, & 0 \le r \le R \\ \frac{1}{4}(1 - r^2) + \frac{R^2}{2}\ln r, & R < r < 1 \end{cases} \qquad (6.9)
$$

Note that u_e is constant in $\Omega^{(1)}$.

In the following we apply the insights gained in the previous chapters to the simplified problem. First we need the weak formulation of the boundary value problem for u in order to apply the differentiation formula (4.13) for domain integrals to both sides of the problem. Then we trace the differentiated weak problem back to its classical

formulation. Solving the resulting ordinary differential equation yields the analytic expression of the shape derivative u'.

Weak Formulation:

The variational formulation of (6.1)-(6.4) writes as: Find $u \in V_0 = H_0^1(\Omega)$ such that

$$a(u,v) = \langle f, v\rangle \qquad \forall v \in V_0 \tag{6.10}$$

with

$$a(u,v) = \int_\Omega \nabla u \cdot \nabla v \; dx \tag{6.11}$$

$$\langle f, v\rangle = \int_\Omega kv \; dx \tag{6.12}$$

with $\int_\Omega = \int_{\Omega^{(1)}} + \int_{\Omega^{(2)}}$, where we already incorporated the interface and boundary conditions (6.2) - (6.4).

6.1.3 Boundary value problem for the shape derivative

Shape differentiation:

In the following, the notation of one domain Ω is used. For the differentiation of the left-hand side (6.11) with respect to the geometry, we define

$$F(x,y,p) = p_1 \cdot p_2. \tag{6.13}$$

With

$$D_{y_1}F = D_{y_2}F = 0 \qquad D_{p_1}F = p_2^T \qquad D_{p_2}F = p_1^T$$

and

$$y = \begin{bmatrix} u \\ v \end{bmatrix} \qquad \text{and} \qquad p = \begin{bmatrix} \nabla u \\ \nabla v \end{bmatrix} \tag{6.14}$$

formula (4.13) gives

$$da(u,v) = \int_\Omega \nabla u' \cdot \nabla v \; dx + \int_\Omega \nabla u \cdot \nabla v' \; dx + \int_\Gamma \nabla u \cdot \nabla v \; v_n \; ds, \tag{6.15}$$

whereas the derivative of (6.12) has the form

$$d\langle f, v\rangle = \int_\Omega kv'\ dx + \int_\Gamma kv\ v_n\ ds. \tag{6.16}$$

Relation (4.12) with $\dot{v} = 0$, integration by parts in (6.15) and equation (6.1) lead to the problem:

$$\int_\Omega \nabla u' \cdot \nabla v\ dx = \int_\Gamma \Big[kv\ v_n\Big]\ ds + \int_\Gamma \Big[\nabla u \cdot nV \cdot \nabla v - \nabla u \cdot \nabla v\ v_n\Big]\ ds, \tag{6.17}$$

which reduces to (see section 5.2)

$$\int_\Omega \nabla u' \cdot \nabla v\ dx = \int_\Gamma \Big[kv\ v_n\Big]\ ds \tag{6.18}$$

with the jump notation introduced on page 12 and Γ denoting the interface between the subdomains $\Omega^{(1)}$ and $\Omega^{(2)}$.

Classical Formulation:

By back-integration by parts we obtain the classical formulation:

$$\begin{aligned}
-\Delta u' &= 0 \qquad \text{in } \Omega && (6.19)\\
u'_1 &= u'_2 \qquad \text{on } \Gamma^{(1,2)} && (6.20)\\
\left[\frac{\partial u'}{\partial n}\right] &= [k\ v_n] \qquad \text{on } \Gamma^{(1,2)} && (6.21)\\
u' &= 0 \qquad \text{on } \Gamma && (6.22)
\end{aligned}$$

which also writes as

$$\begin{aligned}
-\frac{\partial^2 u'}{\partial r^2}(r) - \frac{1}{r}\frac{\partial u'}{\partial r}(r) &= 0,\ r \in [0,1) && (6.23)\\
u'_1(R) &= u'_2(R) && (6.24)\\
\left[\frac{\partial u'}{\partial n}(R)\right] &= [k\ v_n] && (6.25)\\
u'(1) &= 0 && (6.26)
\end{aligned}$$

with $r = \sqrt{x_1^2 + x_2^2}$.

This ordinary differential equation has a known exact solution which can be calculated by hand. Before, we determine the normal component of the velocity v_n.

Normal velocity component:

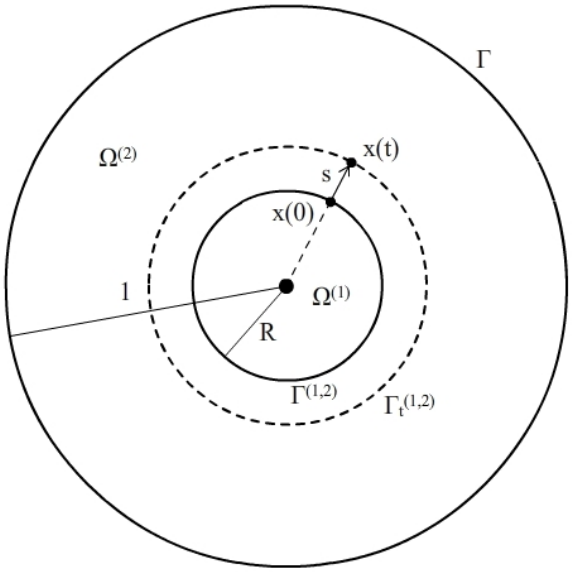

Figure 6.2: Transformation at variation of the radius R

Obviously, if the design parameter R is increased by $t > 0$, the inner circle $\Omega^{(1)}$ grows whereas the outer circle ring $\Omega^{(2)}$ gets thinner in equal measure. The length of the displacement of a particle at position $x(0)$ on the initial interface $\Gamma^{(1,2)}$ to its new position $x(t)$ equals the increase of R, i.e. $s = t$. Therefore we have

$$x(t) = x(0) + t\ n$$

which yields $V(0) = n$ and thus

$$v_n = 1,$$

where n represents the unit outer normal of $\Omega^{(1)}$.

Exact solution u_e':

The exact shape derivative can be expressed as

$$u_e'(r) = \begin{cases} R \ln R, & 0 \le r \le R \\ R \ln r, & R < r < 1 \end{cases} \tag{6.27}$$

Note that the shape derivative u_e', obtained by applying the theory worked out before, equals the derivative of u_e with respect to R, which is reasonable since R identifies the considered design parameter.

6.1.4 The cost functional and its gradient

In this example we do not consider (5.2) but the machine torque (5.6) as cost functional. The exact functional and its derivative with respect to the geometry are given by the exact gradients of u and u', which are obtained from (6.9) and (6.27) by chain rule:

$$\begin{aligned} \nabla u_e(r) &= \begin{pmatrix} \frac{\partial u_e}{\partial r}\frac{\partial r}{\partial x_1} \\ \frac{\partial u_e}{\partial r}\frac{\partial r}{\partial x_2} \end{pmatrix} = \begin{cases} 0, & 0 \le r \le R \\ \left(-\frac{1}{2} + \frac{R^2}{2r^2}\right)\ (x_1, x_2)^T, & R < r < 1 \end{cases} \\ \nabla u_e'(r) &= \begin{cases} 0, & 0 \le r \le R \\ \frac{R}{r^2}\ (x_1, x_2)^T, & R < r < 1. \end{cases} \end{aligned}$$

Inserting into (5.6) yields the following expression for the exact torque:

$$\begin{aligned} T_e &= \frac{1}{\mu_0} \int_{\Gamma_0} \nabla u_e(r)^T Q(x) \nabla u_e(r)\ ds \\ &= \frac{1}{\mu_0} \int_{\Gamma_0} \left[Q(x) \left(-\frac{1}{2} + \frac{R^2}{2r^2}\right) \begin{pmatrix} x_1 \\ x_2 \end{pmatrix} \right] \cdot \left(-\frac{1}{2} + \frac{R^2}{2r^2}\right) \begin{pmatrix} x_1 \\ x_2 \end{pmatrix}\ ds \end{aligned}$$

with $x = (x_1, x_2)$ and Γ_0 denoting the boundary of a circle with fixed radius $R_0 = R + \delta$, $\delta \in \mathbb{R}$, enclosing $\Omega^{(1)}$. However, with the symmetric matrix Q defined in (5.7), the integrand vanishes which leads to

$$T_e = DT_e = 0.$$

Although the numerical computations yield compatible values for T and DT very close to zero, these results are not very significant and do not verify the program. To check the computations anyway, we consider the slightly modified cost functional

$$\begin{aligned} \tilde{T} &= \frac{1}{\mu_0}\int_{\Gamma_0} \nabla u^T \,\mathrm{I}\, \nabla u \; ds \\ &= \frac{1}{\mu_0}\int_{\Gamma_0} |\nabla u|^2 \; ds, \end{aligned} \tag{6.28}$$

which is a functional of the same type as (5.6) (quadratic expression of ∇u). Then, the gradient (5.9) of T changes to

$$D\tilde{T} = \frac{2}{\mu_0}\int_{\Gamma_0} \nabla u \cdot \nabla u' \; ds. \tag{6.29}$$

For the exact functional and its gradient we obtain (w.l.o.g. we take $\mu_0 = 1$)

$$\begin{aligned} \tilde{T}_e &= \int_{\Gamma_0} |\nabla u_e(r)|^2 \; ds \\ &= \int_{\Gamma_0} \left(-\frac{1}{2} + \frac{R^2}{2r^2}\right)^2 (x_1^2 + x_2^2) \; ds \\ &= \int_{\Gamma_0} \left(-\frac{r}{2} + \frac{R^2}{2r}\right)^2 ds \\ &= 2R_0\pi \left(-\frac{R_0}{2} + \frac{R^2}{2R_0}\right)^2 \end{aligned}$$

and

$$\begin{aligned} D\tilde{T}_e &= 2\int_{\Gamma_0} \nabla u_e(r) \cdot \nabla u_e'(r) \; ds \\ &= 2\int_{\Gamma_0} \frac{R}{r^2}\left(-\frac{1}{2} + \frac{R^2}{2r^2}\right)(x_1^2 + x_2^2) \; ds \\ &= \int_{\Gamma_0} \left(-R + \frac{R^3}{r^2}\right) ds \\ &= 2R_0\pi \left(-R + \frac{R^3}{R_0^2}\right). \end{aligned}$$

Again, $D\tilde{T}_e$ equals the derivative of $\tilde{T}_e$ with respect to the design parameter R.

6.1.5 Results

Finally, we compare the numerical computations of the state variable u, its shape derivative u', the (modified) cost functional $\tilde{T}$ defined in (6.28) and its shape gradient $D\tilde{T}$ given by (6.29) with their analytic counterparts calculated above.
From now on, the reduced cost functional $\tilde{T}$ is referred to as cost functional and denoted by T.

Figure 6.3 plots the absolute error between the exact solution u_e, given by (6.9), and the solution u of the variational problem (6.10) in Ω, for $R = 0.2$ and an integration curve defining a circle with radius $R_0 = 0.3$. The difference in Ω between the exact shape derivative u'_e and u' obtained by solving (6.18) is visualized in figure 6.4.

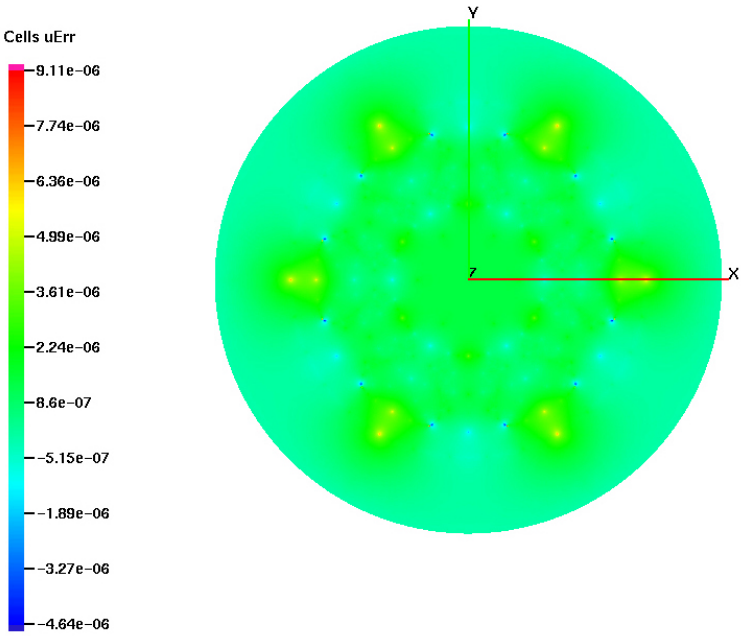

Figure 6.3: Error in the state variable u

The absolute errors plotted in the two figures 6.3 and 6.4 are of order 10^{-6}, where the magnitude of both the state variable u and its shape derivative u' is approximately 10^{-1}, which proves that the computations of u and u' are quite accurate.

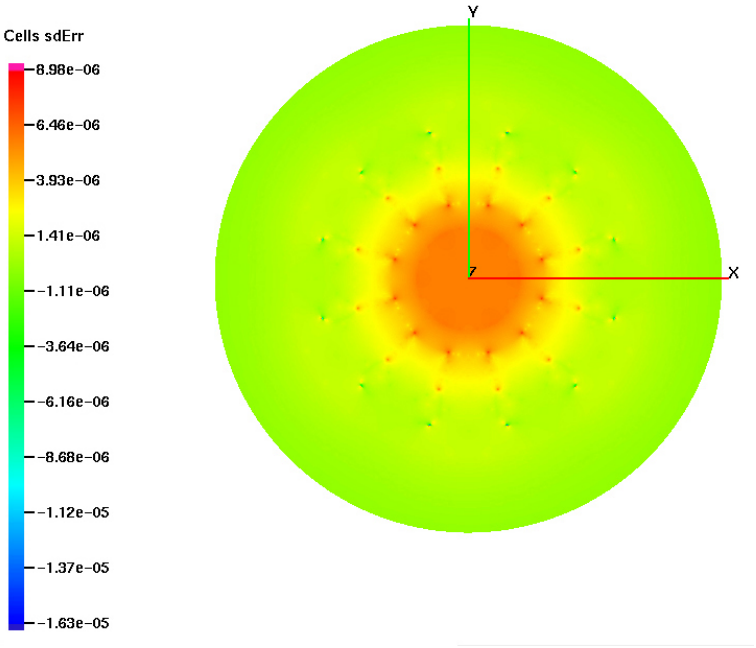

Figure 6.4: Error in the shape derivative u'

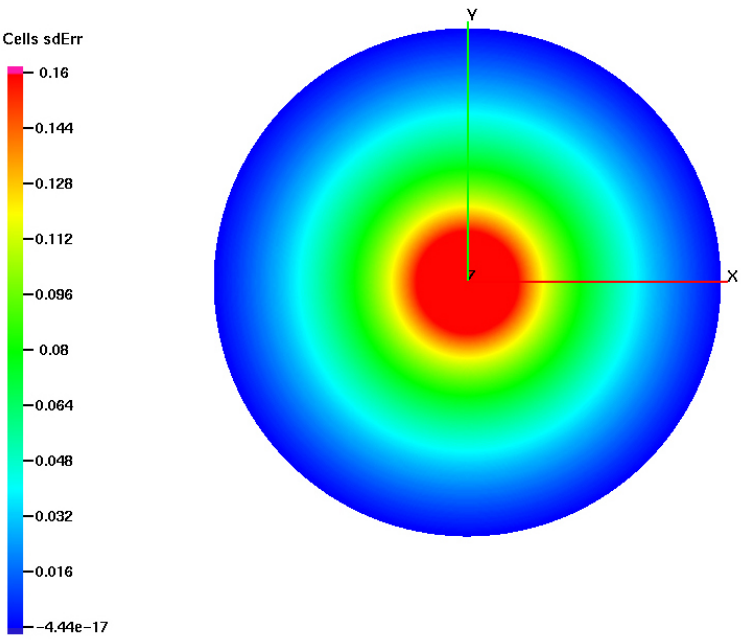

Figure 6.5: Error in the shape derivative u' when the variational problem is not well-defined in $H^1(\Omega)$

Figure 6.5 shows that the error in the shape derivative is large (absolute error and u' are both of order 10^{-1}) , when u' is computed as the solution of the variational problem

$$\int_\Omega \nabla u' \cdot \nabla v \; dx = \int_\Gamma \Big[kv \; v_n \Big] \; ds - \int_\Gamma \Big[\nabla u \cdot \nabla v \; v_n \Big] \; ds,$$

which is obtained by simplifying (6.17) as we at first simplified the variational problem (5.22) in section 5.2. Analogously to (5.23) in section 5.2, the right-hand side of the equation above is not well-defined in $H^1(\Omega)$ and hence, the accuracy of the computed shape derivative cannot be guaranteed. The underlying test example shows that this actually leads to wrong results and points out the importance of the considerations on page 51 to eliminate the troublesome term (5.24) in the variational problem for u'.

Figure 6.6 shows the exact cost functional T_e in comparison with the program output for T for different values of the design parameter R. The integration curve is constantly chosen as circle of radius $R_0 = 0.4$. The red line plots the behavior of the exact torque T_e, the blue dashed line refers to the computed cost functional T.

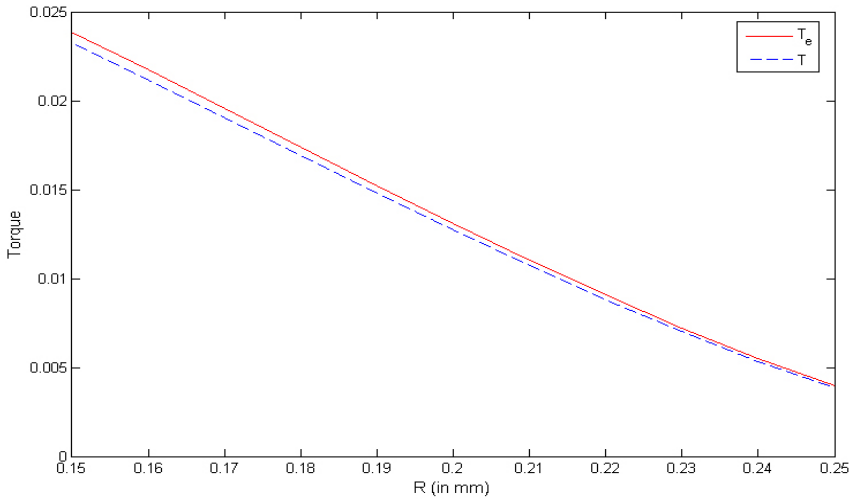

Figure 6.6: Comparison of computed and exact cost functional

Analogously, the difference between the analytic shape gradient DT_e (red line) and the computed one (blue dashed line) is visualized in figure 6.7, which also plots the difference quotient of T by comparison (green dash-dotted line). The error between the

exact and calculated values is very small which suggests the accuracy of the computer program.

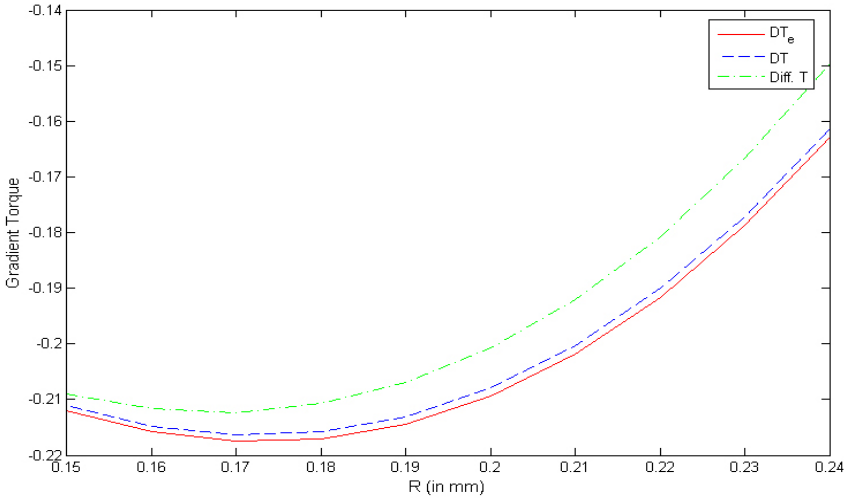

Figure 6.7: Comparison of computed and exact gradient of the cost functional

6.2 Original Problem

Now we concentrate on the original problem, where the curve defining the shape of the cogs is moved as worked out in chapter 3. We restrict the numerical tests to variation of one design parameter, the ratio ρ of the radii of the two tangent circles identifying the cog curve. In other words, the position of the midpoints is constant but the size of the circles changes. The geometric meaning of the resulting shape change was discussed in subsection 3.3.1.

6.2.1 Problem Description

Figure 6.8 shows the division of the motor into several parts in the program of Dr. Clemens Pechstein. It points out the cogs lying in the middle of their coil segments, plotted for the ratio $\rho = 1$. Although each subdomain is dyed in a different

color, this does not mean that all subdomains are made of different materials. The graphic rather illustrates the modelling for the simulation. For instance, the six parts of the outermost circle ring all identify air surrounding the motor.

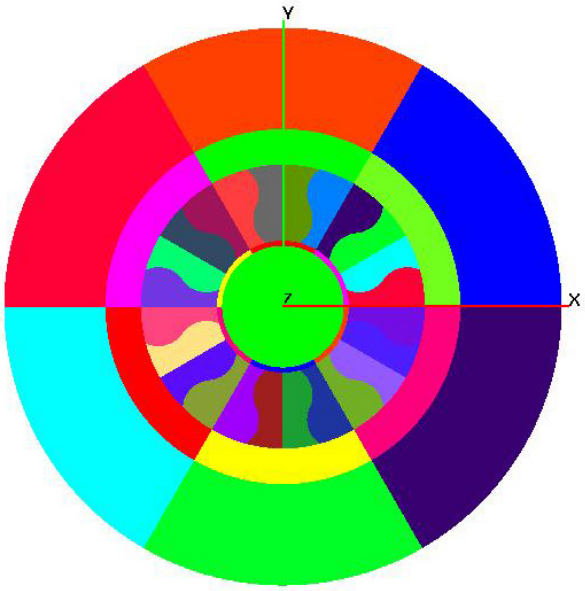

Figure 6.8: Motor subdomains for simulation

The following motor dimensions were chosen (constantly) for the computations:

- rotor radius:	0.012 m
- width of airgap:	0.001 m
- width of coils:	0.015 m
- width of iron ring:	0.007 m
- width of air:	0.02 m

Again, we assume linearity and further simplify the problem by setting $\mu = 1$ everywhere and neglecting the permanent magnetization occuring in the rotor. The current density J_3 is piecewise constant and occurs only in the coil areas A, where the value of J_3 is derived from the given intensity of current I by

$$J_3 = \frac{I}{A}.$$

A is the complementary area to a cog in a coil segment, i.e. the white area in figure 3.4, and is approximated by

$$A = \frac{\pi}{12}\left(R_{out}^2 - R_{in}^2\right), \tag{6.30}$$

where R_{out} and R_{in} denote the outer and inner radii of the circle ring containing the cogs, respectively. Hence, the moving cog curve is the interface between two subdomains of different current density. Figure 6.9 visualizes the current density in the motor that is used for the computations.

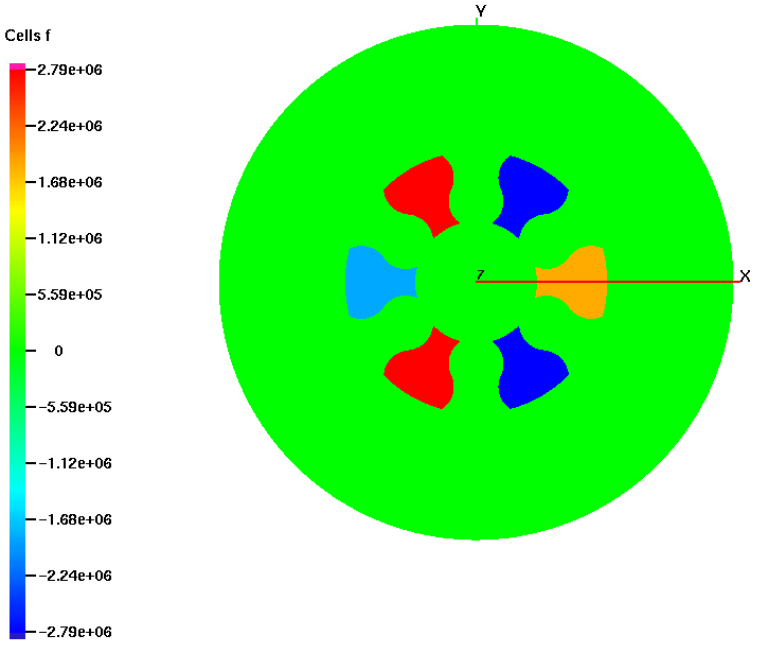

Figure 6.9: Current density in the motor

Since coils of wire are wound around the cogs, the current flows in positive and negative x_3-direction. This leads to different signs of I on either side of a cog. In two neighboring coil areas A among two cogs, the current flow always has the same direction. The magnitude varies between 150 and 300 ampere.

Like in the test problem, we consider the modified torque $\tilde{T}$ as defined in (6.28) as cost functional, which we simply call T. As integration curve in T we fix the outer boundary of the air gap.

6.2.2 Results

The two figures 6.10 and 6.11 plot the solution u of the boundary value problem (2.28) and the shape derivative u', obtained by solving (5.27) with v_n for the parameter ρ, as derived in subsection 3.3.1. The size of the two quantities as well as their occurence in the motor (for J_3 given in figure 6.9) are visualized by different colors.

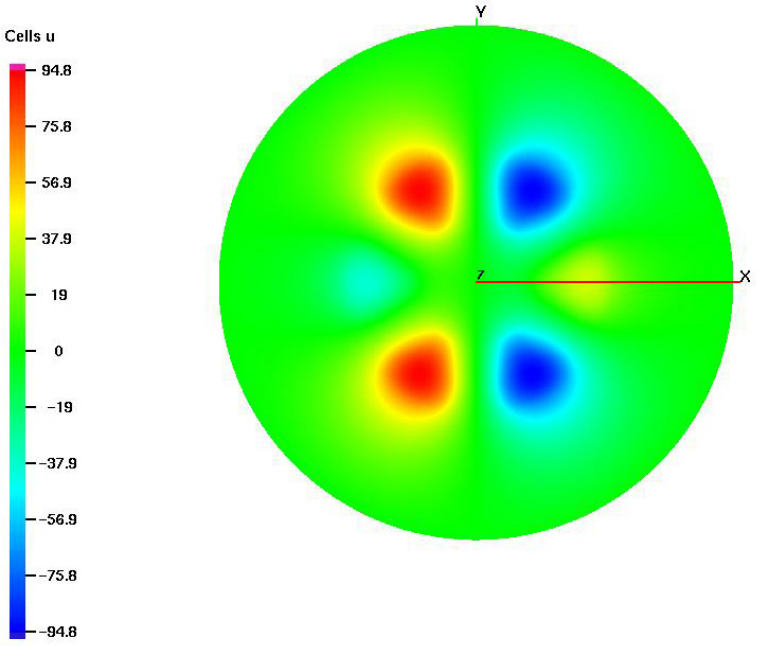

Figure 6.10: State variable u at ratio 1

Figure 6.12 illustrates the behavior of T in the feasible interval of the design parameter ρ. Transparently, the cost functional is monotonically increasing. Thus, for a fixed position of the two tangent circles defining the cog curve, T increases if the outer circle

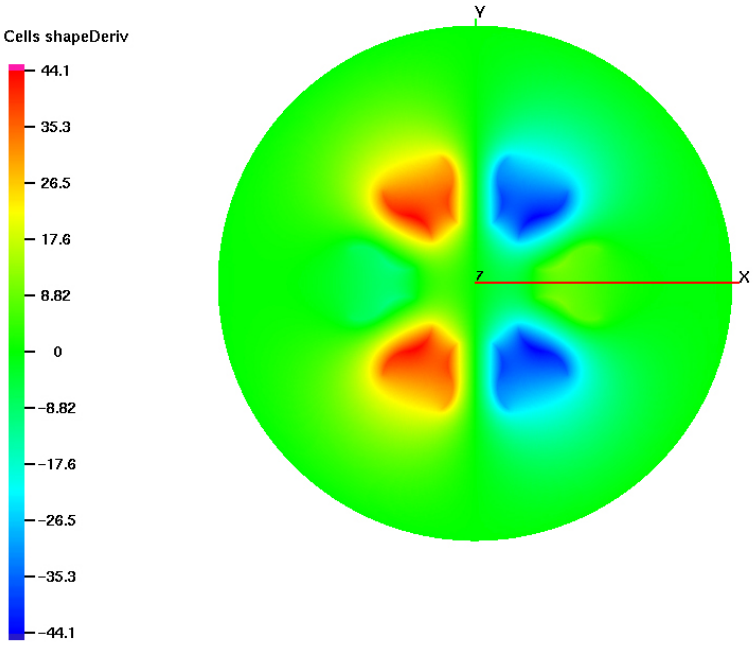

Figure 6.11: Shape derivative u' at ratio 1

(which cuts the iron ring) gets bigger whereas the other circle (which is closer to the rotor) gets smaller. Note that we are interested in the maximum of the functional since we consider T as cost functional instead of $\mathcal{J}$.
In order to produce noticeable modifications in the motor geometry, a rather large stepsize $h = 0.1$ was chosen for the calculations of T. For these steps of ρ in the plotted interval, the relative change in T ranges from 5.8 to 34% and averages 14.2%.

Figure 6.13 compares two different methods to differentiate T with respect to the geometry for values of ρ in the interval $[0.6, 1.5]$ with stepsize $h = 0.1$. The blue dashed line connects the approximations of the derivative of T in the grid points by the forward difference quotient. The corresponding values resulting from the shape derivative approach are plotted by the red line. The plot makes clear that the two curves develop very similarly which confirms that DT makes sense.

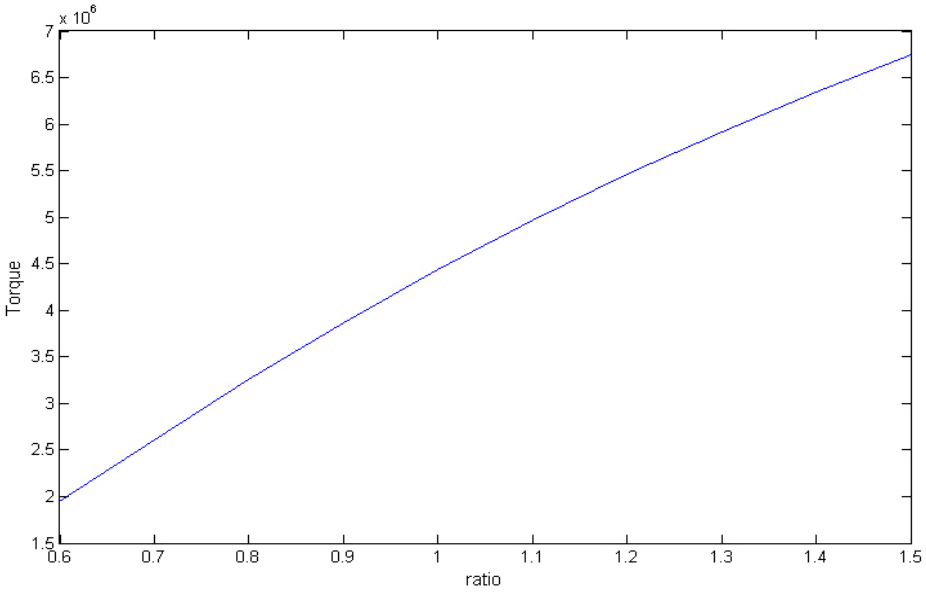

Figure 6.12: Development of the cost functional

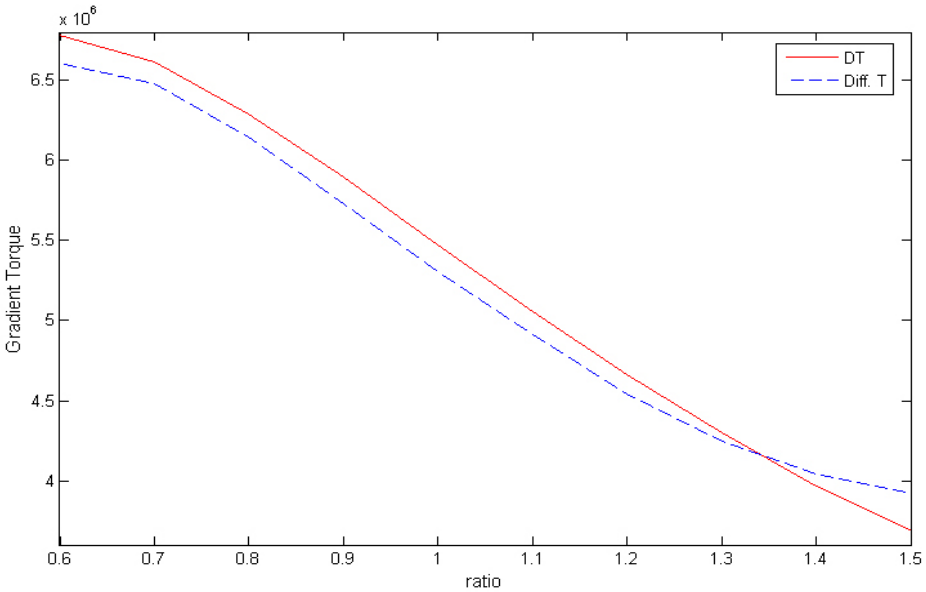

Figure 6.13: Comparison of differentiation methods

Chapter 7

Conclusion and Future Work

The electromagnetic phenomena arising at the simulation of the permanently magnetized synchronous motor led, starting from the Maxwell's equations, to a nonlinear elliptic scalar PDE in $2D$: the PDE constraint of the shape optimization problem. The solution u of the resulting nonlinear BVP was required for the evaluation of the cost functional describing the machine's power output.

Gradient information was not attained by difference quotients, but the cost functional was differentiated with respect to the geometry of the motor, by means of shape derivatives. The meaning of differentiation with respect to the geometry of a body was discussed in detail, the considered changes of the motor domain Ω were visualized. General formulas were derived for the computation of shape gradients of functionals, that consist of domain or boundary integrals, where both the integration area (or curve) and the integrand were dependent on the differentiation variable Ω.

We noticed that the obtained exact shape gradient $D\mathcal{J}$ of the cost functional defined, like $\mathcal{J}$ itself, a function of Ω and u, but additionally depended on u', the shape derivative of u. u' identified the solution of another BVP related to the original one for u. Applying the derived differentiation formulas to all terms of the existing problem for u led to a variational problem with solution u'. The new problem for u' turned out to be linear, in contrast to the BVP that has u as solution.

The numerical tests with ParNFB showed for the constructed test problem with known solution, that the calculations of u and its shape derivative u' were of high accuracy. The computations of the cost functional T and its gradient DT were very close to the exact values T_e and DT_e for all considered values of the design parameter R. The values

obtained by a forward difference quotient of T were similar to the computed gradient DT.
For the original problem where the shape of the cogs is changed, we observed as well that the derivatives obtained by difference quotients and shape derivatives behave similarly.

So far, the computational costs have been equal for both methods because the setting of the considered test problem, as well as the original problem, led to linear problems. But in general, every function evaluation of T is equivalent to solving a nonlinear problem. Computing the difference quotient needs additional function values of T, whereas the calculation of DT only requires the additional solution of one linear problem for each design parameter. Therefore, using the shape derivative approach to determine the gradient of T requires less effort than the computation of difference quotients.
Another advantage of the presented method is that there is no need to choose appropriate stepsizes.
Moreover, the difference quotient approximates the shape gradient of the cost functional, whereas DT represents the exact gradient.

Altogether, the presented method of computing the shape gradient of the cost functional with shape derivatives seems to be a valuable method and shows great promise for shape optimization problems with underlying PDE constraints.

Future work:

This work can be continued in the following directions:

1. *Permanent magnetization and nonlinearity.*
   The results in chapter 6 are obtained for a motor model where the whole rotor consists of linear material and where the permanent magnetization is disregarded. Actually, the rotor is made of nonlinear material, enclosed by a circular ring of permanent magnets as visualized in figure 2.2.

2. *Cost functional.*
   The original cost functional $\mathcal{J}$ given in (5.1) also regards copper losses besides the machine torque T.

Furthermore, computing the torque at different rotor positions (angles) and considering the mean torque, would lead to a more appropriate cost functional.

3. *Variation of other design parameters.*
   The present simulations are all concerned with changes of the ratio ρ. Similar tests could be accomplished for the remaining design parameters, i.e. the coordinates of the circle midpoints. With the Eulerian derivatives for the remaining parameters, the shape gradient would be obtained.

4. *Optimization.*
   The shape gradient $D\mathcal{J}$ derived by the shape derivative approach could finally be used to solve the optimization problem (2.1).

5. *Parameterization*
   The design parameters introduced in chapter 3 describe the cog shape by two tangent circles. One could just as well define parameters that have nothing to do with circles, leading to a completely different cog form.

Bibliography

[1] S. Boisgerault and J.-P. Zolesio. Shape Derivative of Sharp Functionals Governed by Navier-Stokes Flow. In *Partial differential equations: theory and numerical solution*, pages 49–63. Chapman & Hall/CRC, July 1999.

[2] Andreas C. Cangellaris and Yu Zhu. *Multigrid Finite Element Methods for Electromagnetic Field Modeling*. John Wiley and Sons, 2006.

[3] Kyung K. Choi and Nam H. Kim. *Structural Sensitivity Analysis and Optimization: Linear systems, Band 1.* Mechanical engineering series. Springer Berlin, 1 edition, 2005.

[4] M.C. Delfour and J.-P. Zolesio. *Shapes and Geometries: Analysis, Differential Calculus, and Optimization*. SIAM, 2001.

[5] Michel C. Delfour and Jean-Paul Zolesio. Tangential Calculus and Shape Derivatives. *Lecture Notes in Pure and Applied Mathematics*, 216:37–60, 2001.

[6] J. Haslinger and R.A.E. Mäkingen. *Introduction to Shape Optimization: Theory, Approximation, and Computation*. SIAM, 2003.

[7] N. Ida and J.P.A. Bastos. *Electromagnetics and Calculation of Fields*. Springer, 2 edition, 1997.

[8] Arnulf Kost. *Numerische Methoden in der Berechnung elektromagnetischer Felder*. Springer, 1994.

[9] L.D. Landau and E.M. Lifschitz. *Elastizitätstheorie*, volume 7 of *Lehrbuch der theoretischen Physik: in 10 Bänden*. Akademie Verlag GmbH, Berlin, 1991.

[10] Marwan Moubachir and J.-P. Zolesio. *Moving shape analysis and control: applications to fluid structure interactions*. Chapman & Hall/CRC, 2006.

[11] Germar Müller. *Theorie elektrischer Maschinen*. VCH, 1995.

[12] Germar Müller, Karl Vogt, and Bernd Ponick. *Berechnung elektrischer Maschinen*. Wiley-VCH, 6 edition, 2008.

[13] Stephan Schmidt and Volker Schulz. Shape Derivatives for General Objective Functions and the Incompressible Navier-Stokes Equations. Technical Report Preprint-Nr.: SPP1253-10-05, DFG-SPP 1253, February 2009. http://www.am.uni-erlangen.de/home/spp1253.

[14] Jan Sokolowski. Displacement Derivatives of Thin Shells. *Contemporary Mathematics*, 209:247–260, 1997.

[15] Jan Sokolowski and Jean-P. Zolesio. *Introduction to Shape Optimization: Shape Sensitivity Analysis*. Springer Berlin, 1992.

Eidesstattliche Erklärung

Ich, Elisabeth Frank, erkläre an Eides statt, dass ich die vorliegende Arbeit selbstständig und ohne fremde Hilfe verfasst, andere als die angegebenen Quellen und Hilfsmittel nicht benutzt bzw. die wörtlich oder sinngemäß entnommenen Stellen als solche kenntlich gemacht habe.

Linz, am 19. Januar 2010

Elisabeth Frank